We are IntechOpen,
the world's leading publisher of
Open Access books
Built by scientists, for scientists

6,900
Open access books available

186,000
International authors and editors

200M
Downloads

Our authors are among the

154
Countries delivered to

TOP 1%
most cited scientists

12.2%
Contributors from top 500 universities

CLARIVATE ANALYTICS
BOOK CITATION INDEX
INDEXED

WEB OF SCIENCE™

Selection of our books indexed in the Book Citation Index
in Web of Science™ Core Collection (BKCI)

Interested in publishing with us?
Contact book.department@intechopen.com

Numbers displayed above are based on latest data collected.
For more information visit www.intechopen.com

Conjugated Polymer and Hybrid Polymer-Metal Single Nanowires: Correlated Characterization and Device Integration

L. Gence[1], V. Callegari[1], S. Melinte[1], S. Demoustier-Champagne[1], Y. Long[2],
A. Dinescu[3] and J.L. Duvail[4]

[1]*CeRMiN, Université catholique de Louvain, Louvain-la-Neuve*
[2]*College of Physics, Qingdao University, Qingdao*
[3]*National Institute for R&D in Microtechnologies, Bucharest*
[4]*Institut des Matériaux Jean Rouxel, CNRS, Université de Nantes, Nantes*
[1]*Belgium*
[2]*People's Republic of China*
[3]*Romania*
[4]*France*

1. Introduction

More and more in recent years, investigators in industry and academia are taming the structural and electronic properties of conjugated polymer-based nanowires (NWs) and nanotubes (NTs) that display an impressive applicative potential from bio-environmental sensing and energy harvesting to ultra-low power electronic devices and high density memories. Today, the methods used to synthesize conjugated polymer (CP) NWs span from scanning probe lithography [Lim & Mirkin (2002)] and mechanical stretching [He et al. (2001)] to electrospinning [Reneker (2000)] and templated electrochemical [Jerôme & Jerôme (1998); Martin (1994; 1996)] and wetting procedures [Massuyeau (2009)].

Intriguingly, while CPs present vast technological opportunities and can be easily combined to inorganic materials, hybrid metal-CP NWs have been scarcely studied [Gence (2007); Hernandez (2004); Park (2004)]. They can be advantageously produced by high-throughput template strategies that offer a very good control over the composition and spatial distribution of the different NW segments [Duvail (2008); Liang (2002)]. Nevertheless, the use of single hybrid metal-CP NWs in real applications asks for properly identifying their intrinsic behavior. First, this exigency stems from the obvious requirement of tuning their specific properties in post-synthesis and post-assembly technological steps [Jang (2006); Tran et al. (2009); Yoon et al. (2007)]. Second, the unique opto-electronic properties of single hybrid metal-CP NWs are expected to be closely linked to their intricate architecture and to emerge more exquisitely than those of pure CP NWs [Aleshin (2004); Cao (2008); Duvail (2007)].

The aim of this chapter is not to give a complete overview of the literature addressing CP NWs; the focus is on state-of-the-art techniques for synthesizing, characterizing and

integrating hybrid metal-CP NWs. We first present the fabrication of well-shaped and mechanically robust hybrid metal-CP NWs and in the next section we describe the morphology and the microstructure of the resulting NWs. Several advanced techniques such as Raman spectroscopy and electron spin resonance, that enhance our ability to harness promising properties of CP-based NWs, are also presented and discussed. The following section includes research efforts to decrypt electronic properties of CP-based NWs and hybrid metal-CP NWs. Methods for contacting single NWs are reviewed and critically compared. The subsequent section introduces microdevices specially designed for the correlated characterization of single CP-based NWs. The last section refers to the integration and the potential applications of CP-based NWs.

2. Fabrication by the template method

We first address the major issues for preparing well-shaped and mechanically robust hybrid metal-CP NWs and elaborate on a highly reproducible route based upon an all-electrochemical template-based strategy [Reynes & Demoustier-Champagne (2005)].

2.1 Template synthesis

The synthesis of NWs can be achieved by several techniques that can be regrouped into two main families, depending if there are based or not on the use of a template. The template-free method is relatively simple and inexpensive but its control over the morphology and diameter of the NWs is poor compared to the template method [Nalwa (2006); Wan (2008)]. The template method is very efficient for achieving a controlled growth of NWs: the shape, size and orientation of the produced structures are precisely defined by the template [Duvail (2008)]. It allows the synthesis of complex multi-segmented NWs, core-multishell, and coaxial NW structures [Hurst (2006); Kovtyukhova (2004); Lorcy (2009)]. The most used templates are membranes made of ion track-etched polycarbonate (PC) and porous anodic aluminium oxide (AAO); yet, other materials such as Si or polymethylmethacrylate (PMMA) can be used as templates. Typical PC templates [available, for example, at www.it4ip.be] have a mean pore diameter ranging from 30 to 200 nm, pore densities ranging from 10^8 to 10^9 pores.cm^{-2} and thicknesses around 20 μm. Fig. 1(a) gives schematic views of a typical PC template used for synthesizing CP and hybrid metal-CP NWs.

Among the large variety of CPs, three representative species have been included in this chapter: poly[3,4-ethylene-dioxythiophene] (PEDOT), polypyrrole (PPy), and polyaniline (PANI). These CPs are by far the most extensively studied as they exhibit remarkable properties such as environmental stability, interesting redox behavior and the ability to exhibit high electrical conductivities [Sadki (2000)]. While the polymerization of these CPs can be performed by both chemical and electrochemical reactions, the electrochemical polymerization is well adapted for the synthesis within templates. Furthermore, multi-segmented NWs [e.g. combining CP segments with noble (Au, Pt) or transition (Ni, Co metal blocks] can be easily produced using an all-electrochemical process, just by changing the plating solution and adapting the parameters of the deposition of each segment [Callegari (2009); Chung (2005)].

A crucial point of the electrochemical synthesis of the CPs within a template is that, depending on the synthesis parameters, NWs or NTs can be obtained [Cho & Lee (2008);
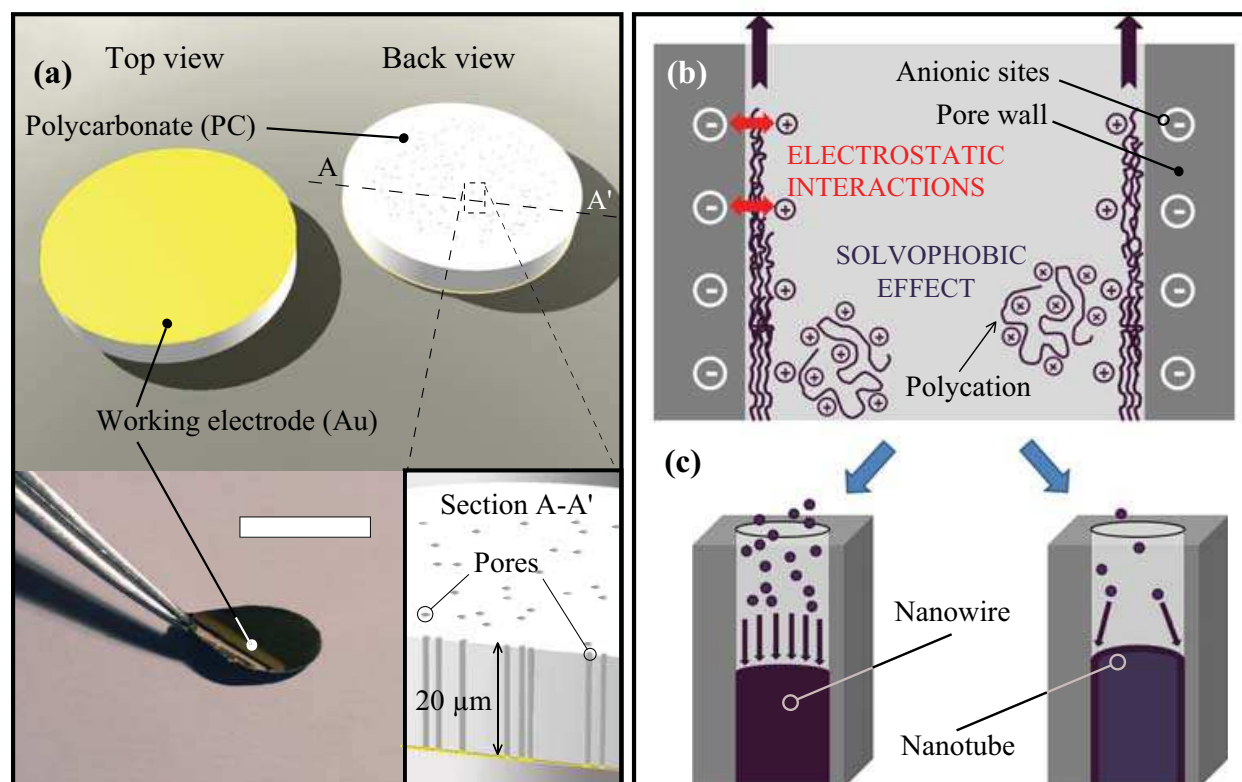
Fig. 1. (a) Top and back views of a flexible PC template used for synthesizing nanowires. In the left inset, the scale bar represents 5 mm. (b) Scheme of the growth mechanism for polymer NTs and NWs within a single pore. (c) Usual relations between synthesis conditions and morphology: Fast reaction rate and insufficient monomer supply lead to NTs. Slow reaction rate and sufficient monomer supply direct NWs.

Xiao (2007)][see Fig. 1.(b)]. While CP NTs could be interesting for different applications such as energy storage or drug release, NWs are needed for obtaining hybrid multi-segmented NWs with good metal-CP electrical interfaces. As revealed in the sequel, the determination of the exact geometry of metal-CP interfaces requires correlated scanning electron microscopy (SEM) and transmission electron microscopy (TEM) investigations.

The mechanism behind the two possible geometrical configurations is still matter of debate. For explaining the growth of nanotubes inside a template, it has been proposed by Martin and coworkers [Martin (1994; 1996)] that solvophobic and electrostatic interactions between CPs and the template occur within the pores of the template, favouring thus the tubular geometry [see Fig. 1.(b)]. A recent study [Xiao (2007)] has shown that the morphological transition between the two configurations can be explained by a mechanism based on monomer diffusion and reaction kinetics. Roughly, as exemplified in Fig. 1.(c), a slow polymerization reaction performed in presence of a sufficient monomer supply leads to the formation of NWs, while a faster reaction associated to an insufficient supply of monomer produces preferentially produces NTs.

2.2 Pure PEDOT and hybrid tri-segmented Au-PPy-Au NWs

Here, we briefly present the synthesis of pure PEDOT NWs and detail the fabrication of hybrid metal-CP NWs, taking the case of a tri-segmented Au-PPy-Au NW. Specifically, the

3,4-ethylenedioxythiophene (EDOT) monomer was provided by Bayer AG and used as received. The polymerization bath was an aqueous solution, previously developed by Sakmeche and coworkers [Sakmeche (1996)], containing 0.07 M sodium dodecylsulfate, 0.1 M $LiClO_4$ and 0.05 M EDOT.

A schematic view of tri-segmented NW synthesized by an all-electrochemical method is given in the Fig. 2.(a). The synthesis is performed by three sequential electrodepositions. The first step consists in the electrodeposition of a gold segment by cyclic voltammetry (CV). A cyanide free solution containing 0.1 M KCl, 0.1 M K_2HPO_4 and 0.03 M $HAuCl_4.3H_2O$ (Acros) in deionized (DI) water could be used [Reynes & Demoustier-Champagne (2005)]. The electrodeposition is achieved by cycling the potential from 0.7 to 0 V at a typical scan rate of 200 mV.s^{-1}. Figure 2.(b) gives a cyclic voltammogram recorded during the deposition of the first gold segment within a 100 nm pore diameter PC template. The typical growth rate is about 5 nm.s^{-1}. It is important to notice that the gold electrodeposition rate is highly dependent on the pore diameter and decreases with increasing the pore diameter. The second, PPy segment can be deposited into the pores by the electropolymerization of the pyrrole. The synthesis of PPy onto noble metal segments (Au, Pt) could be realized via CV by sweeping the potential from 0 to 0.85 V. A common electrolyte is an aqueous solution containing 0.1 M $LiClO_4$ and the monomer (5 to 100 mM range). In some cases, 7×10^{-4} M sodium dodecyl sulfate is added and used as surfactant. Figure 2.(c) gives the cyclic voltammograms corresponding to the deposition of the PPy segment at the first (full curve) and 200th cycle (dashed curve). Then, the third Au segment is electrodeposited under similar conditions to those used for the first segment. As shown in the Fig. 2.(d), a drastic change of the CV curve shape, accompanied by a strong increase of the current, indicates that deposition overflows the nanopores. This allows to detect easily the end of the synthesis. After the synthesis of each NW segment, the sample is rinsed in DI water for at least 30 minutes in order to remove the remaining plating solution left inside the pores of the membrane.

Remarkably, the resulting metal-PPy-metal NWs are characterized by two morphologically different metal-PPy interfaces as revealed by TEM observations and schematized in the insets of the Fig. 2.(a). The metal-onto-PPy interface is mechanically more robust than the PPy-onto-metal interface thanks to a higher adhesion surface. Several strategies have been envisaged to improve the mechanical strength of these interfaces. First, we optimized electrochemical parameters for the growth of the Au-onto-PPy interface by systematically investigating the effects of the potential sweep rate and the monomer concentration on its mechanical strength [Gence (2007)]. Concerning the bottom PPy-onto-Au interface, as its morphology cannot be modified just by playing on electrodeposition parameters, its mechanical strength could be enhanced by increasing the adhesion between the two different materials. Among the different possible strategies, we first investigated the use of self-assembled alkylthiol monolayers (SAMs) onto gold [Lahav (2006)]. We used 11-mercaptoundecanoic and 3-mercaptopropionic acids. The SAM is inserted between the gold and the PPy segment to create an electrostatic bond between the negatively charged carboxylate groups of the chemisorbed monolayer and the positively charged growing polycation as shown in the Fig. 3.(a). On top of the 11-mercaptoundecanoic acid SAM no CP growth has been observed. This is probably due to the presence of long aliphatic chains that passivated the Au segments. Unfortunately, even if the CP growth occurred on the thinner chemisorbed SAM (3-mercaptopropionic acid), no qualitative improvement of the

mechanical strength has been detected upon this chemical modification of the interface. Nevertheless, the modification of interfaces by the use of SAMs is essential for the synthesis of hybrid transition metal-CP NWs.
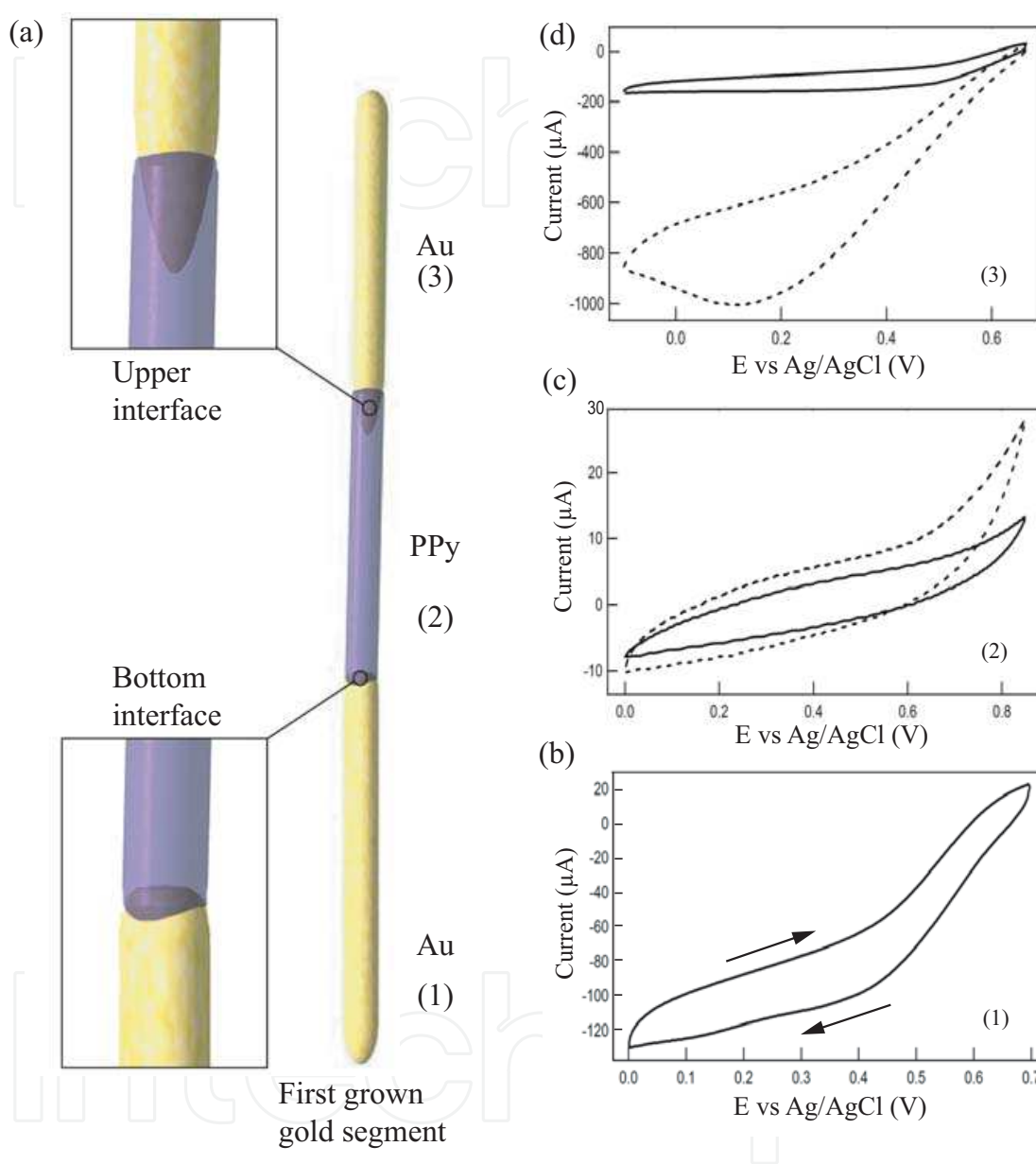

Fig. 2. (a) Schematic view of a tri-segmented Au-PPy-Au nanowire. The insets are magnified views of both polymer-metal interfaces. (b-d) Typical cyclic voltammograms obtained for the synthesis of each nanowire segment. (b) Cyclic voltammogram collected during the deposition of the first gold segment. (c) Cyclic voltammograms recorded during the deposition of the PPy segment. First cycle (full curve) and 200th cycle (dashed curve) are given. (d) Cyclic voltammograms acquired during the deposition of the third grown gold segment before (full curve) and after overflowing (dashed curve).

2.3 Hybrid NWs with transition metals

The synthesis of bi- and tri-segmented NWs including transition metals is now described. Bi-segmented, transition metal-onto-CP NWs can be easily elaborated by changing the electrochemical bath. While reducing the metal ions on top of the CP segment, the CP cannot be dissolved. Yet, it can be reduced, thus exhibiting a lower doped level state. The reverse sequence, i.e. the electropolymerization of usual CPs on transition metals, including Ni and Co, is less straightforward to achieve. Indeed, the oxidation potentials of these metals are much lower than the one of conjugated monomers and thus, dissolution of the metal occurs before electropolymerization begins. Figure 3.(c) gives typical chronoamperograms for the electrodeposition of Co and Ni segments. The length of the
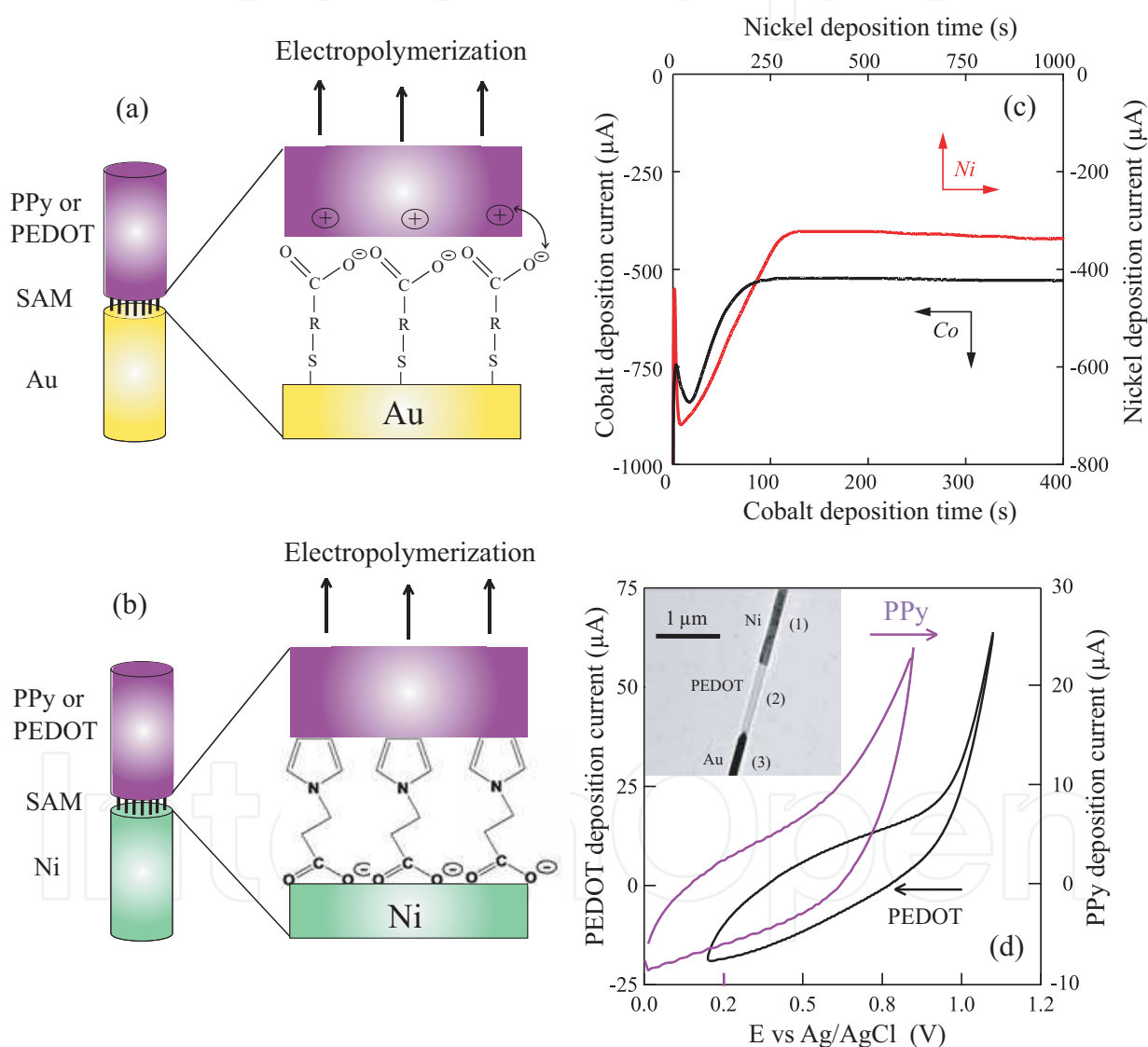

Fig. 3. (a, b) Schematic views of the modified metallic (Au, Ni) interfaces using SAMs. In the case of Ni (b), the presence of the SAM improves the electropolymerization process. (c) Typical chronoamperograms for the electrodeposition of Co (Ni) NW segments. (d) Cyclic voltammograms recorded during the deposition of PPy (PEDOT) segment on top of the first grown Ni segment modified by a SAM. The inset displays a typical 110 nm diameter Ni-PEDOT-Au NW as seen by TEM.

transition metal segments can be easily controlled by the electrodeposition time: the growth rates for Ni and Co, observed for 110 nm diameter NWs, are 0.5 and 0.7 μm.min^{-1}. Specifically, the Ni segment could be electrodeposited by chronoamperommetry at −1.05 V from an electrochemical bath containing Ni sulfate hexahydrate ($NiSO_4.6H_2O$) and boric acid (H_3BO_3), while Co is electrodeposited from a solution containing cobalt sulfate heptahydrate ($CoSO_4.7H_2O$) by applying a constant potential of -0.95 V.

Towards preparing hybrid transition metal-CP NWs, a major problem to overcome is to suppress or limit the metal re-dissolution at the oxidative potential required for the electrodeposition of the CP. It is therefore necessary to find synthesis conditions that will strongly passivate the metal without impeding electropolymerization. Our approach consists in the use of a SAM. The 3-(Pyrrol-1-yl) propanoic acid has been chosen due to its facile synthesis and because it contains two end-functional groups, a carboxylate group at one extremity and a pyrrole group at the other end, that can specifically interact with the Ni substrate and the growing CP, respectively [see Fig. 3.(b)]. Prior to the electrodeposition of the CP, the SAM is deposited by immersion of the PC template containing the Ni segment in a 3-(Pyrrol-1-yl) propanoic acid solution for more than 18 hours. The CP segment (PPy or PEDOT) could be then synthesized by CV using standard electrodeposition parameters. Typical cyclic voltammograms recorded during the deposition of the second, (PPy or PEDOT) segments on top of the first grown Ni segments modified by SAMs are given in Fig. 3.(d). In order to fabricate tri-segmented nanowires, a third metallic block can be synthesized on top of the CP segment, by CV (e.g. Au) or by chronoamperommetry (e.g. Co). Following this procedure, 100-nmdiameter Ni-(PPy or PEDOT)-Au and Ni-(PPy or PEDOT)-Co NWs have been successfully synthesized. The inset to the Fig. 3.(d) gives an example of a 100-nm-diameter Ni-PEDOT-Au NW as observed by TEM: the first grown Ni segment is clearly distinguishable. Despite the use of the 3-(Pyrrol-1-yl) propanoic acid SAM, the percentage of unbroken NWs containing transition metal segments remains low compared to the tri-segmented NWs containing only noble metals.

3. Structural characterization

In this section, we present the morphology of several classes of CP NWs, including pure PEDOT NWs and hybrid metal-CP NWs, as studied by SEM, TEM, atomic force microscopy (AFM), Fourier transform Raman spectroscopy and electron spin resonance (ESR).

The morphology of PEDOT NWs is captured in SEM and AFM images reported in Fig. 4.(a, c, d) and Fig. 4.(b), respectively. Once the PC membrane has been removed, PEDOT - as well as other CP NWs - tend to cluster into bundles because of their long length and flexibility. This behavior is reinforced by the NW anchoring on the bottom metallic electrodes (see below). This is an important point to take into account for the integration of CP NWs into devices as well-separated NWs or NTs can be required for high-sensitivity applications. The unambiguous discrimination between NW bundles and large diameter NWs can be easily obtained via AFM studies; the AFM image Fig. 4.(b) reveals five closely-packed PEDOT NWs. In this case, the diameter is determined from the height shift to avoid the convolution by the tip which has to be considered when measuring the lateral size. Finally, a SEM study is not sufficient to determine whether NWs or NTs have been fabricated for given synthesis conditions. As an example, a TEM investigation has shown that the template electropolymerization of PEDOT under the conditions described above results in the
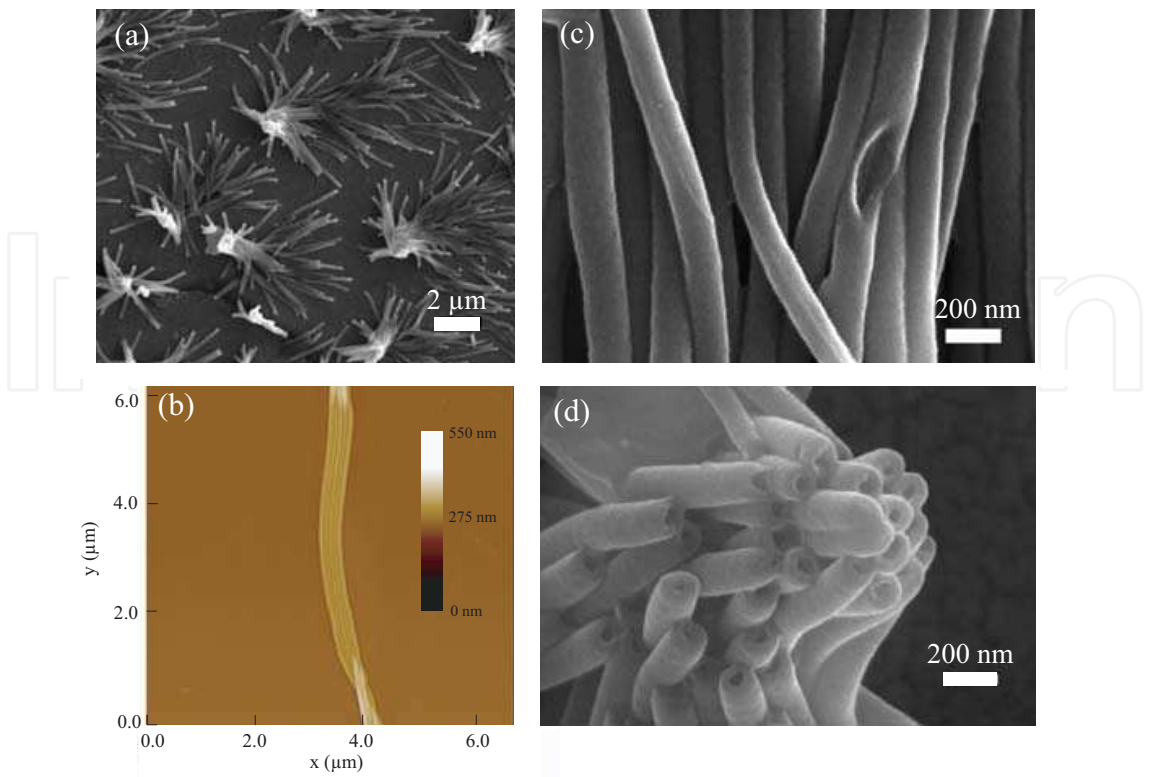
Fig. 4. Morphological characterization of PEDOT NWs after the removal of the PC template. (a) SEM picture of 3−4 μm long NWs. (b) AFM topography image of a rope of NWs. (c) SEM image revealing 100-120 nm diameter NWs. (d) SEM view of a standing up bundle of NWs.
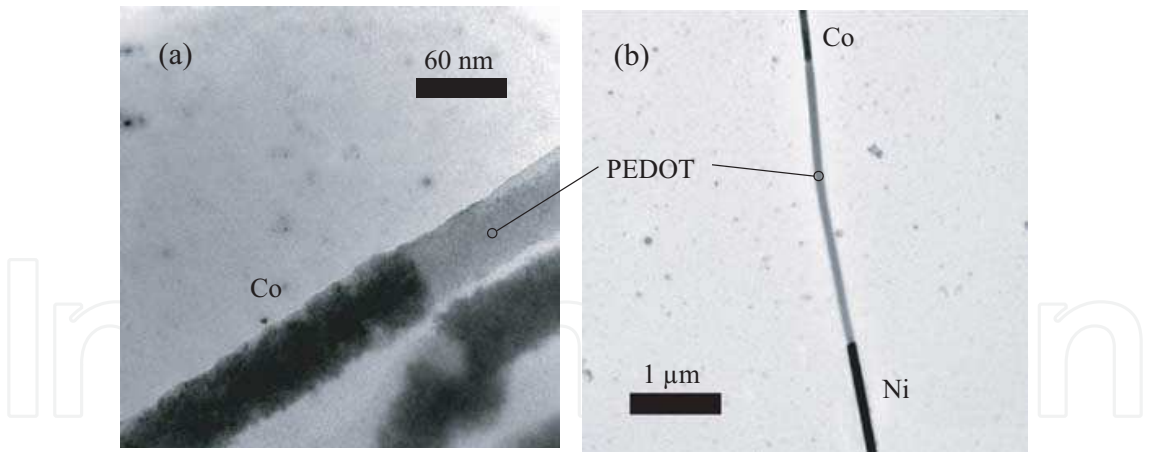

Fig. 5. (a) TEM picture of a 60 nm diameter Co-onto-PEDOT NW. (b) TEM picture of a 100 nm diameter tri-segmented Ni-PEDOT-Co NW.

fabrication of PEDOT NWs, while the opened top-ends of the synthesized nano-objects, observed by SEM [Fig. 4.(b)], suggest NTs. In the case of hybrid metal-CP NWs, the metal and CP segments are unambiguously distinguishable by SEM and TEM without any particular contrasting treatment. For example, in a classic SEM picture, tri-segmented metal-(PPy or PEDOT)-metal NWs appear composed of a dark polymer segment inserted between two bright metal segments. In TEM micrographs (Figs. 5 and 6), the polymer block appears more transparent than the metallic segments, due to its lower electronic density.
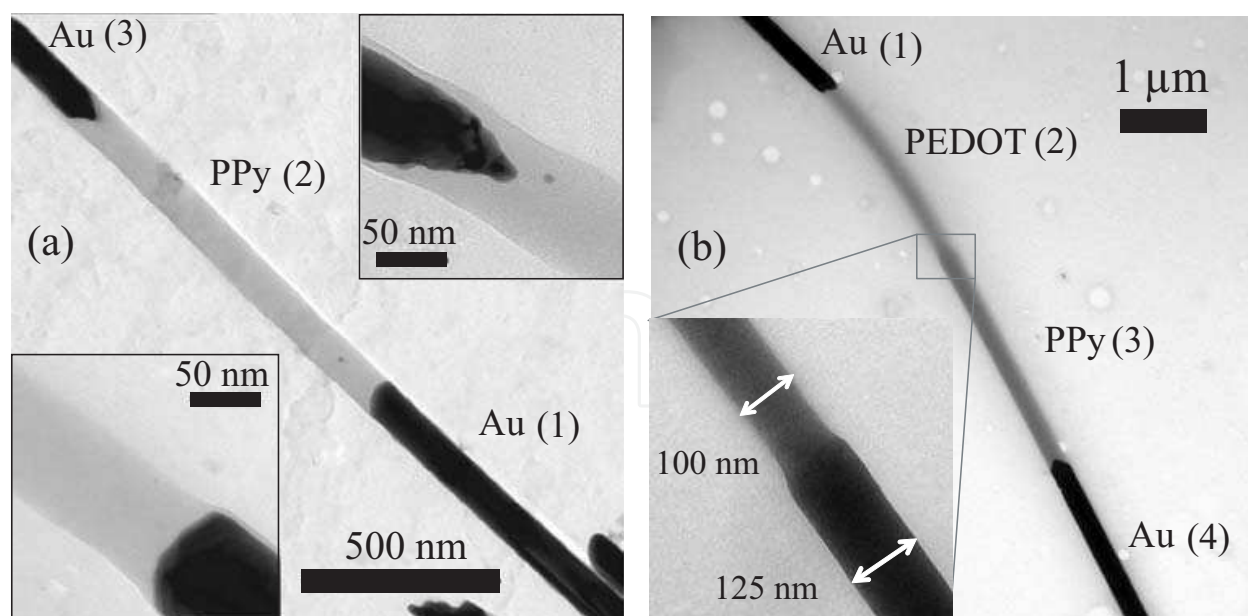
Fig. 6. (a) TEM image of the two Au-PPy interfaces in Au-PPy-Au NWs. The lower and upper insets give closer views of the PPy-onto-Au (first grown) and Au-onto-PPy (second grown) interfaces. (b) TEM picture of a 110 nm diameter tetra-segmented Au-PEDOT-PPy-Au NW. The inset shows a zoom of the polymer heterojunction.

Figure 6 presents TEM images of tri- and tetra-segmented metal-CP NWs. As displayed in the two insets of Fig. 6.(a), the fabricated Au-PPy-Au NWs have two morphologically different Au-PPy interfaces. In terms of mechanical robustness, the PPy-onto-Au [referred as (1)] interface is smoother and more fragile than the Au [referred as (3)]-onto-PPy interface. Figure 6.(b) illustrates typical Au-PEDOT-PPy-Au NWs. During the synthesis, for enhancing the overall mechanical robustness of the NWs, the deposition sequence was determined according to careful observations on the shape and strength of the different Au-CP interfaces. The PEDOT block was first deposited on the Au segment, as the strong chemical bond between Au-S compensates for the weakness of the flat interface. The PPy block was then electrodeposited onto the PEDOT segment, the strength of the metal-onto-PPy interface being ensured by its meniscus shape. The inset to Fig. 6.(b) gives a magnified view of the PPy-onto-PEDOT heterojunction. It appears that the PEDOT segment shrank more than the PPy segment during the solvent evaporation in a sampling process.

Another unique characterization tool for CP-based NWs is Fourier transform Raman spectroscopy. In the past, the influence of the diameter (35, 75, 100 and 150 nm) on the PEDOT structure was studied on electrodeposited NWs at +0.80 V. All spectra were recorded with an excitation line at 676 nm after dissolution of the membrane [Fig. 7.(a)]. The bands located at 1424 cm^{-1} and at 1495 cm^{-1} are attributed, respectively, to the symmetric and antisymmetric C=C vibrations of the thiophene rings. Interestingly, the intensity ratio $I(1495\ \mathrm{cm}^{-1})/I(1424\ \mathrm{cm}^{-1})$ increases significantly when the diameter decreases. This variation has been attributed to an increase of the conjugation length when the NW diameter decreases [Duvail (2004)]. Additional information on the nature of the charge (polaronic, bipolaronic) carriers could be obtained from ESR studies. Figure. 7.(b) compares room temperature ESR spectra of PEDOT NWs (accomodated into PC membranes) with diameters approximately equal to 200, 100, and 50 nm (as measured by SEM) and normalized
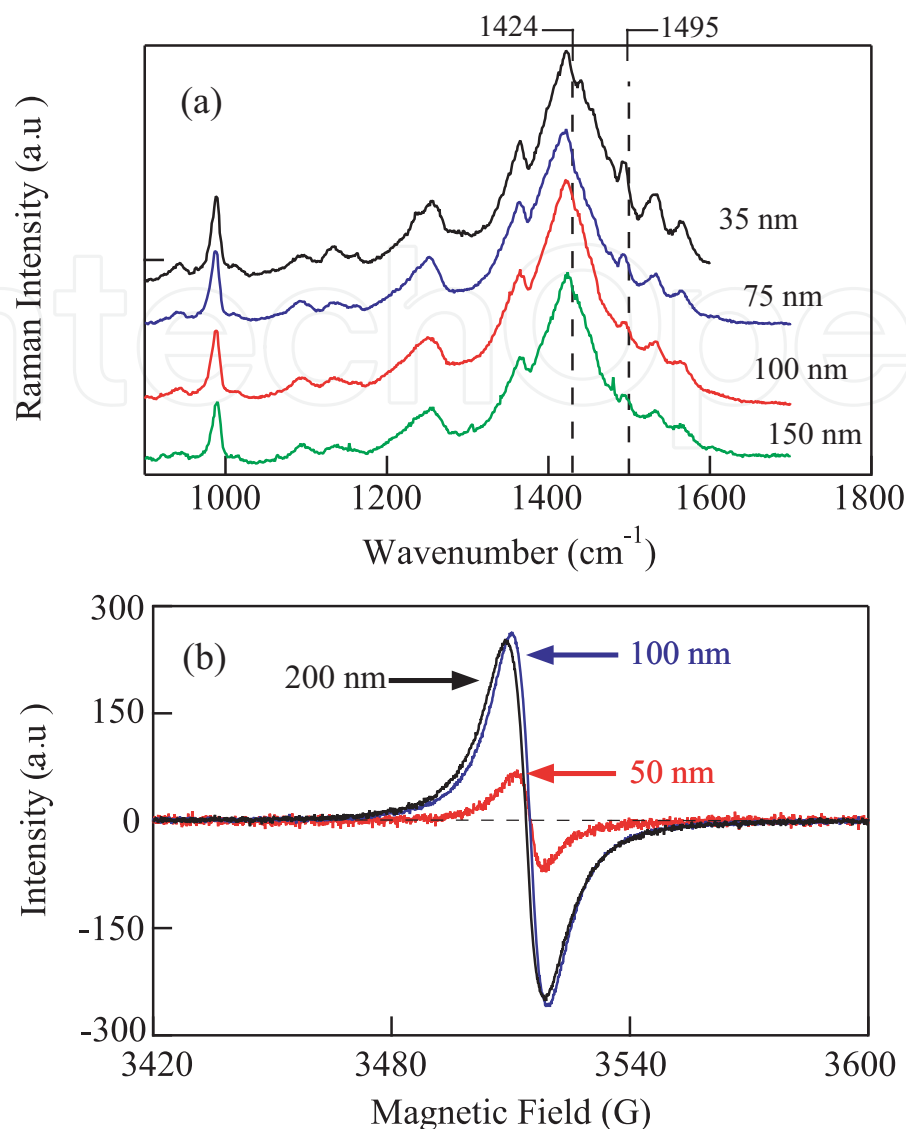
Fig. 7. (a) Effect of the PEDOT NW diameter on the Raman spectra (λ_{exc} = 676 nm). Curves are shifted for clarity. (b) ESR spectra (f_{exc} = 9.4 GHz) of PEDOT NWs.

to the same EDOT mass. A quantitative analysis of the Lorentzian-like peaks (directly proportional to the spin density) has been carried out. Subsequently, these results have been correlated to the doping level of the NWs estimated from XPS data [Duvail (2004)], revealing that the bipolarons are the dominant charge carriers in these NWs and their contribution increases when the diameter decreases. This conclusion corroborates Raman studies and suggests a strong molecular and supermolecular improvement when the NW diameter decreases.

4. Electrical properties

In this section, we review different techniques for contacting NWs grown by the template method and compare their limitations and advantages. The electrical characterization can be performed in a vertical configuration with multiple NWs contained within the template or in a planar configuration, with NWs freed from the template and dispersed on a substrate.
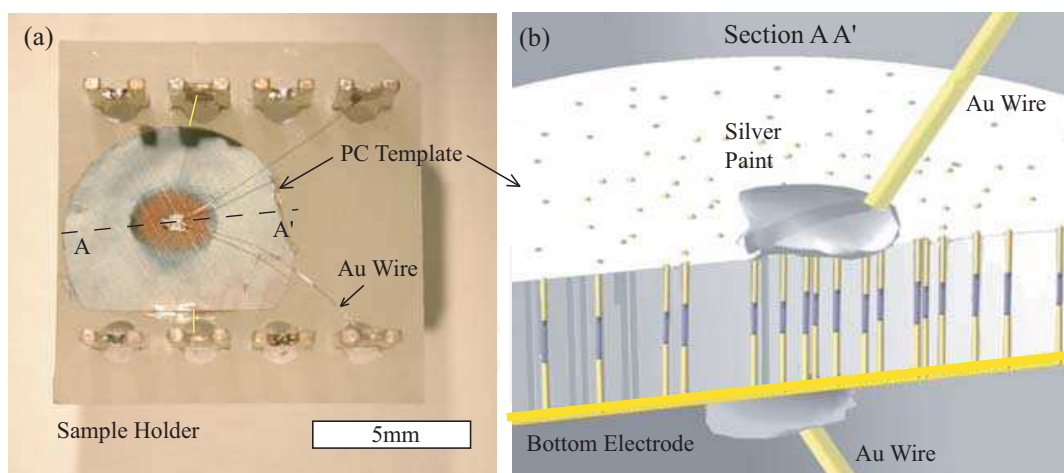
Fig. 8. (a) Optical micrograph of multiple NWs contacted in a vertical configuration within the PC template. (b) Schematic view (for tri-segmented NWs) of the section AA' defined in the panel (a).

4.1 Vertical contacting techniques

The vertical configuration is quite convenient and has been frequently employed those last years for the electrical and thermal characterization of NWs [Duvail (2002); Heremans (2002; 2003); Gence (2008); Lorcy (2009)] as it is very fast and requires no complex processing of the sample to be measured. Figure 8.(a) gives an optical micrograph of a PC template mounted on a sample holder and electrically contacted immediately after the electrochemical synthesis. The NWs enclosed within the template are mechanically supported by the PC membrane and are protected from the effect of both oxygen and ambient humidity [Chtanko (2004)]. However, four main drawbacks arise from this method. First, the exact number of connected NWs is not known. An estimation of the number of connected NWs can be made from the porosity of the template and the surface of the electrical contact. The typical values of porosity and hand-made contact surface are 10^9 pores/cm^2 and 5×10^{-4} cm^2. Assuming that all pores are filled, this results in a typical number of connected NWs of about 5×10^5. Among this huge number of NWs, by taking into account the calibration of the synthesis parameters, one expects a wide distribution of the physico-chemical characteristics. This distribution results in an averaging effect on the electrical measurements and contributes in masking the intrinsic properties of single NWs. Second, the length of each segment can differ quite significantly between different NWs prepared in the same PC membrane. As the diameter can differ slightly (10 - 20%) from one NW to the other, the intrinsic conductivity (calculated by using the geometrical parameters) can vary by a factor of 2. Third, the resulting two-contact geometry can not avoid the contact resistance to be included in the measurements, in contrast to the four-contact geometry. Fourth, the measurement of multiple NWs contained within a template does not allow any interaction of the NWs with the environment or with any chemical, electrical or physical agent. For all the above reasons, the use of NWs freed from the template is the best choice for the characterization of their intrinsic properties. For application-oriented purposes, the integration of NWs with microelectromechanical systems or electronic devices is required and the NWs have to be precisely aligned and positioned onto microfabricated contacts. Fortunately, various techniques have been specifically developed for the assembly of single NWs onto electrodes [Cao (2008)] and many others are under close scrutiny.
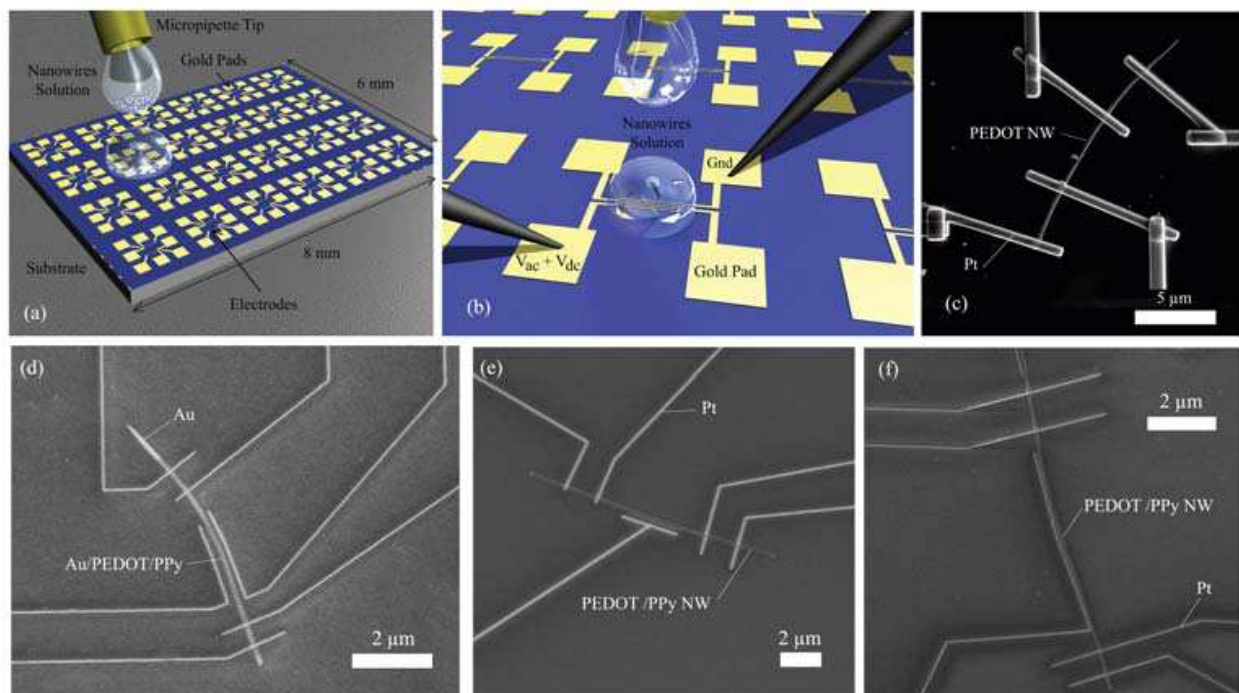
Fig. 9. (a) Schematic 3D view of an electrical device designed for integrating the NWs by a bottom contact approach. (b) Zoom on a single NW deposition assisted by an external electric field. (c-f) SEM micrographs of CP NWs connected by the top contact approach: (c) FIB and (d-f) EBID techniques.

4.2 Planar contacting techniques

For planar contacting techniques, the NWs have to be gently freed from their matrix and the first step consists in the removal of the working electrode from the back of the templates. Generally, the working electrode is made of a few hundred nm Au layer that can be etched with iodine solutions. The PC templates are easily dissolved in dichloromethane, while AAO templates require typically NaOH solutions. The techniques used for contacting single NWs in planar configurations [see Fig. 9.(a)] can be divided in: (i) bottom-contact methods (where NWs are deposited on top of predefined electrodes) and (ii) top-contact methods (where the electrodes are deposited on top of the NWs). In both cases, the substrate includes a high quality insulating layer (Si_3N_4 or SiO_2). For the bottom-contact method, metallic (Au, Pt) electrodes are defined on this top insulating layer by photolithography or electron-beam lithography (EBL). Figure 9.(a) gives a schematic 3D view of a typical device designed for integrating NWs by the bottom-contact method via dropcast deposition. Dielectrophoretic trapping of NWs [see Fig. 9.(b)] has been known for a long time [Smith (2000); Dong (2005)] and used very recently for the precise alignment of hybrid metal-CP NWs in solution [Park (2004); Cao (2008)]. For the top-contact approach, typically, EBL and related methods are employed for the definition of the electrodes on top of the NWs. For example, Pt electrodes could be directly deposited by electron beam induced deposition (EBID) or by focused ion beam (FIB) on top of the NWs [Duvail (2007); Shen (2006)]. Micrographs of CP and hybrid metal-CP NWs contacted by Pt electrodes fabricated via FIB and EBID depositions are given in Fig. 9.(c) and Fig. 9.(d-f), respectively.

The main advantage of the top-contact approach is to allow chemical and physical cleaning of NW-electrode interface which is not possible for bottom-contacted NWs. Indeed, in the bottom-contact approach, once the NW is deposited onto the electrodes and after the solvent has dried, some PC residues, previously dissolved in the solution are left on the substrate. These residues, when present at the NW-electrodes interfaces, can alter dramatically the electrical contact between the deposited NW and the electrodes in a non reproducible way and cannot be controlled by any treatment. On the other hand, in the framework of the top-contact approach, the NW-electrodes interfaces can be rinsed in pure solvent repetitively for many hours. Another possibility is to use a short cleaning oxygen plasma before the deposition of the electrodes (Au or Pt) for lift-off processing. Nevertheless, the main drawbacks of the direct writing techniques are the likely modification of the intrinsic doping of the NWs (e.g. dedoping associated to EBID manipulation and additional doping during FIB integration). Specifically, for the bottom-contact approach, the expected physisorption of the CP NWs on the metal electrodes can induce a significant contact resistance to inject charge current with a possibly non-ohmic behaviour. The opposite case is met for FIB top-contacts. The ion implantation, although it is reduced by careful choice of experimental parameters, results quite systematically in ohmic contacts. As a consequence, the Pt lines deposited by FIB have to be separated by typically 2 μm or more to avoid overlapping of the surrounding residual carbon-based deposit. Concerning contacts made by EBID on top of CP NWs, our attempts generally failed to get reliable ohmic contacts.

4.3 Electrical properties of pure PEDOT NWs

The motivation for measuring isolated NWs instead of arrays of NWs comes from the opportunity to determine unambiguously the conductivity σ through a four-probe geometry. Figure 10.(a) gives the diameter dependence of σ at room-temperature for pure PEDOT NWs. An increase by a factor 50 in σ is evidenced when the diameter decreases from 190 to 25 nm. This result confirms the tendency generally reported for arrays of template-synthesized CP NWs. The T-dependence of the resistivity ρ, normalized by $\rho(300 \text{ K})$, for PEDOT NWs with different diameters is shown Fig. 10.(b). The diameter appears to induce dramatic differences in the electrical behaviour. The resistivity ratio $\rho(20 \text{ K})/\rho(300 \text{ K})$, a useful empirical parameter for quantifying the extent of disorder, is reported as a function of the diameter in the inset to Fig. 10.(b). A decrease by a factor about 100 takes place when the diameter decreases from 190 to 35 nm. A precise analysis of the T-dependence of the resistivity has shown that the 190 nm diameter NWs are in an insulating regime (three-dimensional Mott variable range hopping), the 100 nm diameter NWs are in the critical regime of the metal-insulator transition and the 35 nm ones are on the metallic side of the transition. According to correlated investigations of the molecular and supermolecular ordering and the doping level (by Raman spectroscopy, electron spin resonance and X-ray photoelectron spectroscopy), the insulating-to-metal transition has been attributed to a strong structural improvement when the NW diameter decreases [Duvail (2004; 2007)]. The mechanisms responsible for this remarkable structural improvement are most likely the presence of anionic sites at the nanopore surface and the enhanced role of the solvophobic effect when the (electro)polymerization is confined at nanoscale, as initially proposed by C. R. Martin [Martin (1994; 1996)]. However, for NW diameters smaller than 35 nm, the resistivity ratio increases by four orders of magnitude. Interestingly, the electron conduction in the 25 and 30 nm NWs follows the Efros-Shklovskii law. This result suggests that electron-electron interactions play an important role for the charge transport at low T in CP NWs [Aleshin (2004)].
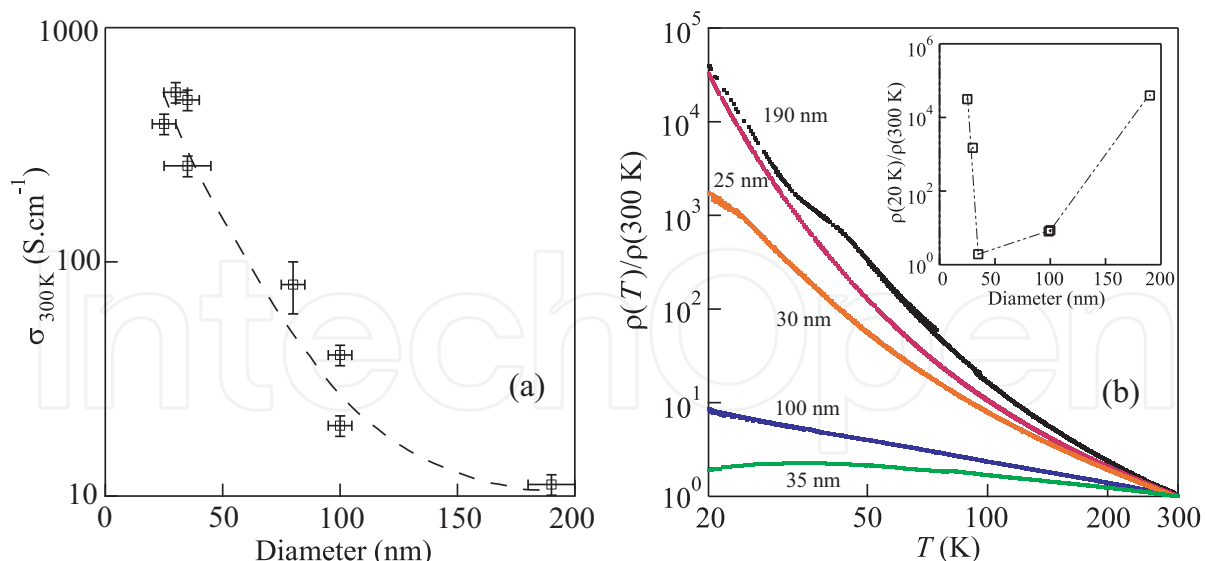
Fig. 10. (a) Diameter dependence of the room-temperature conductivity of PEDOT NWs. (b) Log-Log plot of the temperature dependence of the resistivity (normalized by the room T resistivity) of PEDOT NWs. The inset gives the diameter dependence of the resistivity ratio ρ(20 K)/ρ(300 K).

4.4 Electrical properties of hybrid tri-segmented NWs

We next present electrical transport data for hybrid Au-PPy-Au NWs. The current-voltage $I - V$ spectroscopy is a powerful technique to gain insight into various transport phenomena such as tunnelling and rectification [Aleshin (2004); Gence (2007; 2008)]. Typical current-voltage $I - V$ characteristics are given in Fig. 11.(a-c) for different tri-segmented Au-PPy-Au NWs with diameter ranging from 40 to 160 nm at room and low temperature T. In all samples, the $I - V$ plots are symmetrical and show no rectification effect. For samples with diameter $\phi \geq 50$ nm, the $I-V$ characteristics are ohmic between room temperature and approximatively $T \approx 120$ K. As shown in Fig. 11, the non-linearity of the $I - V$ curves increases with decreasing T, signaling that a peculiar conduction mechanism occurs at very low temperatures [Long (2005)]. Noteworthy, for the 40 nm samples the ohmic region extends down to much lower temperatures $T \approx 25$ K. The resistance values $R(T)$ are obtained from the $(dI/dV)^{-1}$ values at zero bias. For all investigated samples, the resistance monotonically increases with decreasing T, indicating that PPy has a non-metallic behavior. This is coherent with the room temperature conductivity of ≈ 0.04 S.cm^{-1} and it is comparable to the bulk insulating PPy prepared under the same conditions.

Several experimental studies have shown that the Mott variable-range-hopping (VRH) regime is an appropriate model of charge transport in CP NWs as it is well-known for bulk CPs [Aguilar-Hernández & Potje-Kamloth (1999); Park (2004); Bufon (2005)]. In this model, the charge transport is due to thermally activated tunneling among states that are localized in a constant density of states [Mott & Davis (1979)]. In the VRH model, the resistance follows the relation $ln[R(T)] \propto (T_0/T)^{1/(d+1)}$, where T_0 is the Mott temperature and d is the dimensionality of the system. The best fits to our data have been obtained with $d = 3$ [see Fig.11.(d and e)]. This suggests that the three-dimensional (3D) VRH is the appropriate model of transport for tri-segmented Au-PPy-Au NWs.

The peculiarity of the ϕ = 40-nm-diameter tri-segmented NWs can be highlighted using the empirical parameter $R_R = R(77\ K)/R(290\ K)$. This parameter has been frequently used to characterize the extent of disorder in CPs such as PPy or PEDOT [Yoon (1994); Duvail (2007)]. In Fig.11.(f), we have plotted the parameter R_R as a function of the diameter for different NWs. The parameter R_R is found to be four orders of magnitude smaller for the 40 nm diameter samples than for the 70 nm diameter specimens. This suggests that the ϕ = 40 nm Au-PPy-Au NWs exhibit a dramatically lower extent of disorder compared to higher diameter tri-segmented NWs. Moreover, it indicates that the resistance of the PPy-Au junctions can be neglected, at least when measured at temperatures down to 77 K.
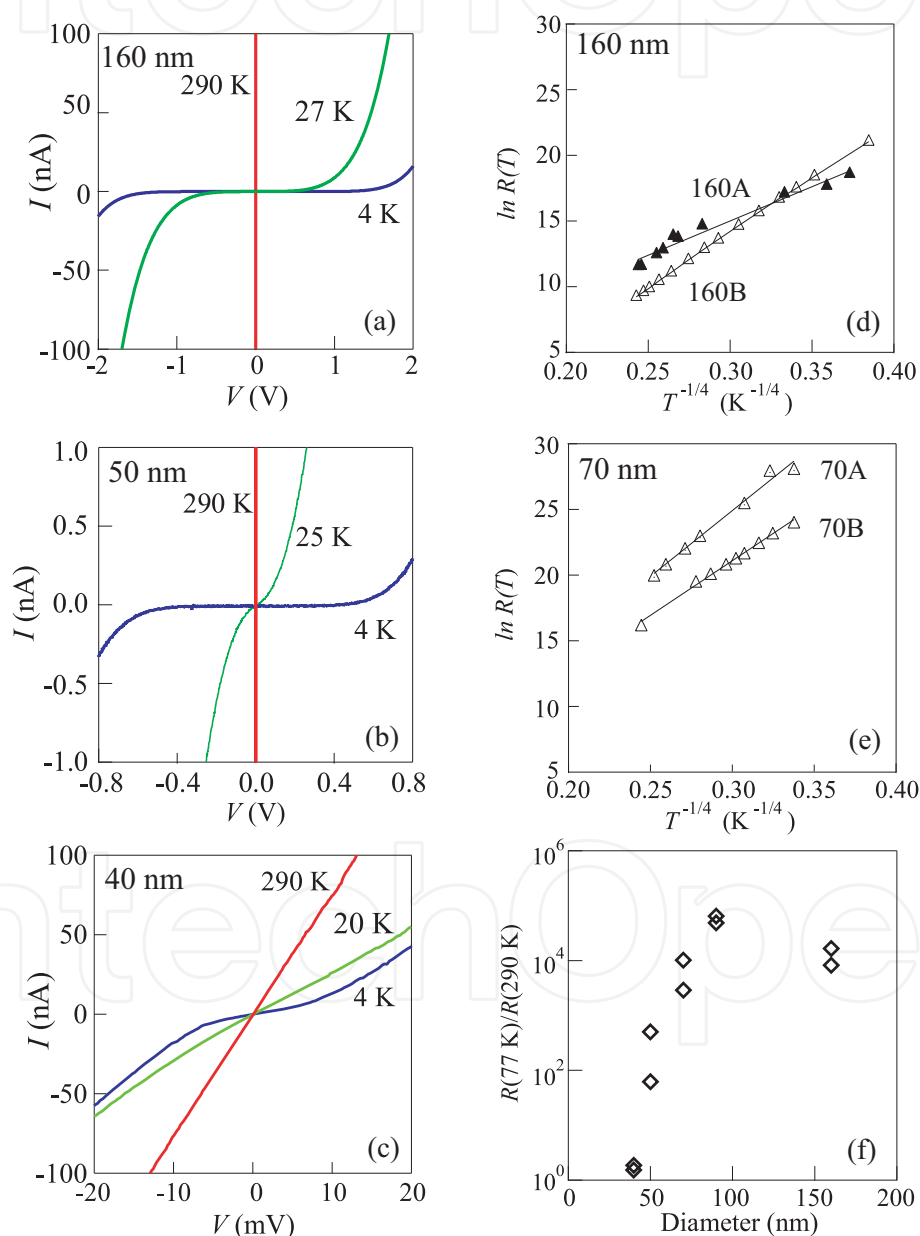

Fig. 11. (a-c) $I − V$ characteristics of tri-segmented Au-PPy-Au NWs with diameters of 160, 50 and 40 nm. (d-e) 3D-VRH plots for 160 and 70 nm diameter samples. The solid lines are the 3D-VRH fits to the data. (f) Diameter dependence of the resistance ratio R_R observed for tri-segmented Au-PPy-Au NWs.

4.5 Tunable electronic behavior of hybrid metal-CP NWs

Hybrid metal-CP NWs are attractive candidates for nanodiodes and transistors [Pinto (2003); Park (2004); Merlo & Frisbie (2004); Pinto (2009)] as well as photonic [Guo (2008); Camposeo (2009)] and electrochromic devices [Cho & Lee (2008)]. This high applicative potential comes from the fact that they make profit from intrinsic properties of CPs (low-cost, flexibility, environmental stability, high biocompatibility) concomitantly with other properties stemming from their low-dimensionality (large surface-to-volume ratio and enhanced properties compared to bulk materials). In particular, the literature data show clearly the current interest towards the engineering of novel CP-based NW devices with tunable electronic properties. We present here a new class of tetra-segmented Au-PEDOT-PPy-Au NWs able to switch their electrical characteristics in function of the redox state of the two CP blocks. To illustrate the principle, we use a chemical treatment performed by immersing the samples in a 0.5 M aqueous solution of $FeCl_3$ for 1 h. We contrast the behavior observed for the tetra-segmented NWs to that observed for tri-segmented NWs.

Figures 12.(a) and 12.(c) give schematic view of tri-segmented (Au-PEDOT-Au) and tetra-segmented (Au-PEDOT-PPy-Au) NWs, respectively. The $I - V$ characteristics of a tri-segmented NW have been measured in a four-probe configuration, before and after $FeCl_3$ treatment, and are given in Fig. 12.(b). The $I - V$ curves are symmetrical and linear. While
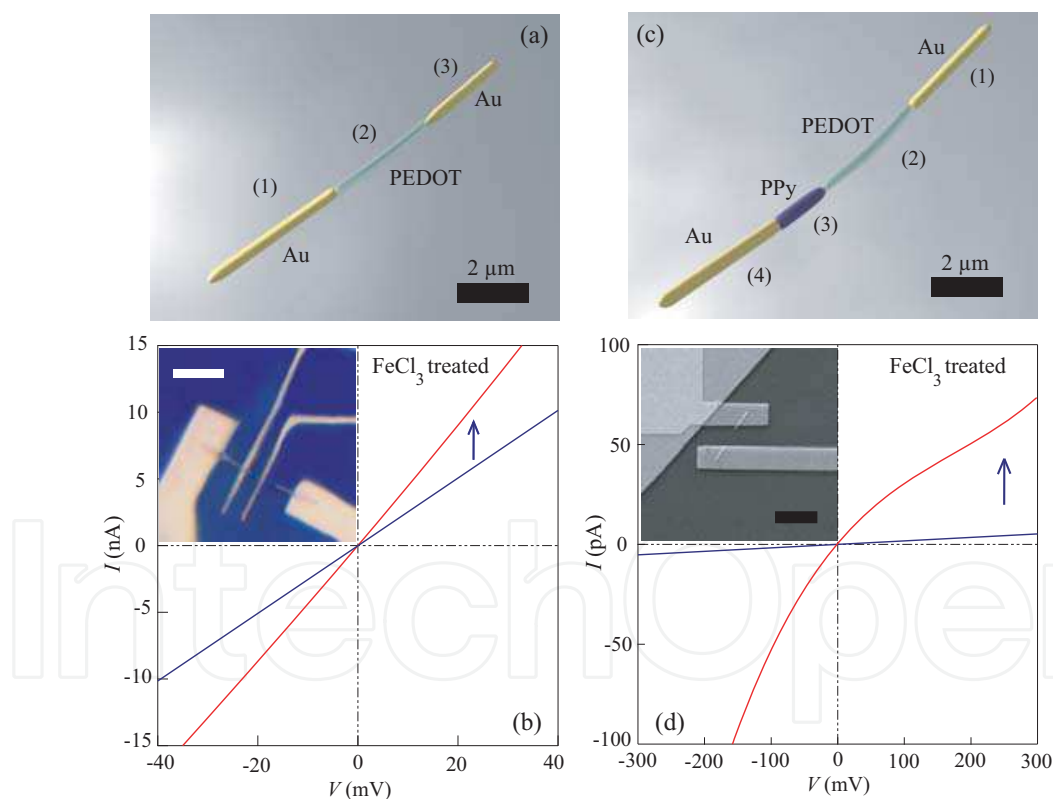

Fig. 12. (a) Schematic view of a tri-segmented Au-PEDOT-Au NW. (b) Four-point $I - V$ characteristics of a single tri-segmented Au-PEDOT-Au NW before (blue curve) and after (red curve) $FeCl_3$ treatment. The inset shows the four probe configuration used for contacting the tri-segmented NW. The scale bar is 5 μm. (c) Schematic view of a tetra-segmented Au-PEDOT-PPy-Au NW. (d) Corresponding $I - V$ characteristics before (blue curve) and after (red curve) $FeCl_3$ treatment. The inset shows a typical tetra-segmented device and the scale bar is 5 μm.

the blue curve corresponds to the as-synthesized NW, the red curve has been obtained after *FeCl*₃ treatment. The observed increase of electrical conductivity of the PEDOT segment could be understood by a shift in the dopant anion equilibrium within the PEDOT [Callegari (2009)]. The chloride ions inserted during the chemical treatment effectively adjust the low dimensional carrier hopping network on the backbone of the polymer inducing an enhanced charge transport.

Similarly to Au-PEDOT-Au NWs, we performed the same experiment with Au-PEDOT-PPy-Au NWs. Remarkably, after the chemical treatment, tetra-segmented NWs exhibit a highly nonlinear $I - V$ characteristic (red curve), accompanied by a current increase. Furthermore, the $I - V$ curve is asymmetric, i.e. the gain of current depends on the sign of the bias voltage: roughly, the gain is enhanced by a factor of 2 at negative bias compared to positive bias. These observations recall the behavior of other types of hybrid NWs that have been proposed in the literature as innovative structures for chemical sensing.

5. Correlated characterization

The correlation of multiple analyses performed on the same, well-defined multi-segmented NWs could lead to a deeper understanding of their structure-function relationships. The aim of this section is to present microdevices specially designed for the correlated characterization of single hybrid metal-CP NWs but it could obviously be applied to other class of hybrid NWs such as hybrid inorganic NWs [Wang (2004)]. We address here the NWs assemblies with membrane-based micro-electromechanical systems. While structural analysis are performed by combining SEM, TEM and AFM microscopies, the microstructure and the elemental composition are investigated by selected area electron diffraction (SAED) and energy dispersive X-ray spectroscopy (EDS) measurements.

5.1 Platforms for correlated characterization

We have used Si micromachining techniques for batch-producing devices based on Si_3N_4 membranes on top of which are deposited the NWs to be analyzed. They are compatible with both bottom and top-contact planar approaches for contacting single NWs (see section 4.2). Figure 13.(a) gives the schematic view of these membrane-based platforms. The relatively small dimensions of the devices are designed for compatibility with various sample holders for correlated characterization. Essentially, 200 *μm*-thick Si wafers are oxidized and a 80 nm-thick low pressure chemical vapor deposition Si_3N_4 layer is then deposited. Afterwards, 100 *nm* thick Au pads are defined by optical lithography. Openings in the nitride layer on the back side of the wafer are created by a double side alignement photolithography followed by dry etching of the exposed areas. Membranes are then released by an anisotropic etching of the Si all through the wafer. The top-contact planar approach is often preferred for device integration, as it allows custom design of the electrodes for each addressed NW. As an example, Fig. 13.(b) gives a topographic AFM image of a single PEDOT NW connected in a transistor configuration. Naturally, in the case of NW transistors, the use of membrane-based devices could allow a comprehensive study of the accord between their structural characteristics - as observed by correlated analyses (TEM, micro Raman, AFM, SAED) - and the measured transistor performances such as the on/off current ratio, the threshold voltage or the gate leakage current [Lieber & Wang (2007)].
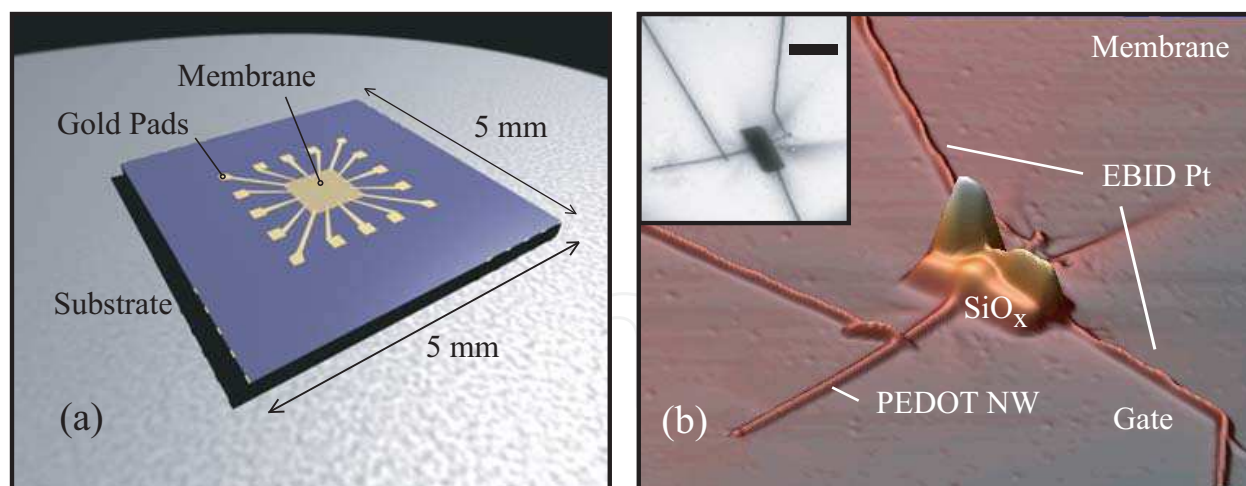
Fig. 13. (a) 3D schematic view of a membrane-based device. (b) AFM image of a single PEDOT NW connected in a transistor configuration on top of a membrane-based device. The *Pt* and *SiO$_x$* elements have been produced by electron-beam induced deposition. The inset is a TEM image of the same NW. The scale bar is 2 *μm*.

5.2 Correlated analysis of hybrid tetra-segmented NWs

A better demonstration of the correlated characterization is offered by hybrid metal-CP NWs. A TEM picture of a Au-PEDOT-PPy-Au NW deposited on top of a *Si$_3$N$_4$* membrane and connected with multiple electrodes is given in the Fig. 14.(a). The geometries of both metal-CP interfaces have been determined by high magnification TEM (not shown here). By the shape of the menisci and the diameter of the segments, it is often possible to guess the nature of the CP blocks. The precise knowledge of the respective positions of the PPy and PEDOT segments in tetra-segmented NWs is important for understanding their subtle electronic behavior, as exemplified in the section 4.5. This identification can be established by EDX spectroscopy. Figure 14.(c) shows EDS spectra recorded on the four spots marked in Fig. 14.(a). Because these spectra have been recorded on top of a *Si$_3$N$_4$* membrane, they all contain peaks at *K* and *L* X-ray emission energies corresponding to Si and N [Bearden & Burr (1967)]. Interestingly, the spectra reveal the presence of S atoms, characteristic for PEDOT, only in the spot III, while the presence of chlorine is identified in spots I and II. The positions of the PEDOT and PPy segments can thus be distinctly determined.

The panel (b) to Fig. 14 gives SAED patterns taken at four different positions on the device. While the SAED obtained through the *Si$_3$N$_4$* membrane and the Au electrodes exhibit the expected amorphous and polycristalline patterns, the PEDOT and PPy both display amorphous patterns. This component of the correlated characterization tool box gives important information about the polymer chain organization of the produced CP segments. Polycristalline structures have been observed recently for PPy and PEDOT NWs synthesized electrochemically [Wang (2007); Lee (2008)]. Hence, the data acquired from the SAED operation of suspended membrane platforms accommodating hybrid metal-CP NWs can be crucial for further optimization of the CP segments' morphology. Figure 15 presents the four probe *I* − *V* characteristics of different segments of a Au-PEDOT-PPy-Au NW contacted with several electrodes (A to F) and shown in the Fig. 15.(b). The respective values for the electrical conductivity are estimated from the *dI*/*dV* values at zero bias. The low value of the conductivity σ_{CD} = 0.2 mS/cm, deduced for the segment CD, is in agreement with the rather
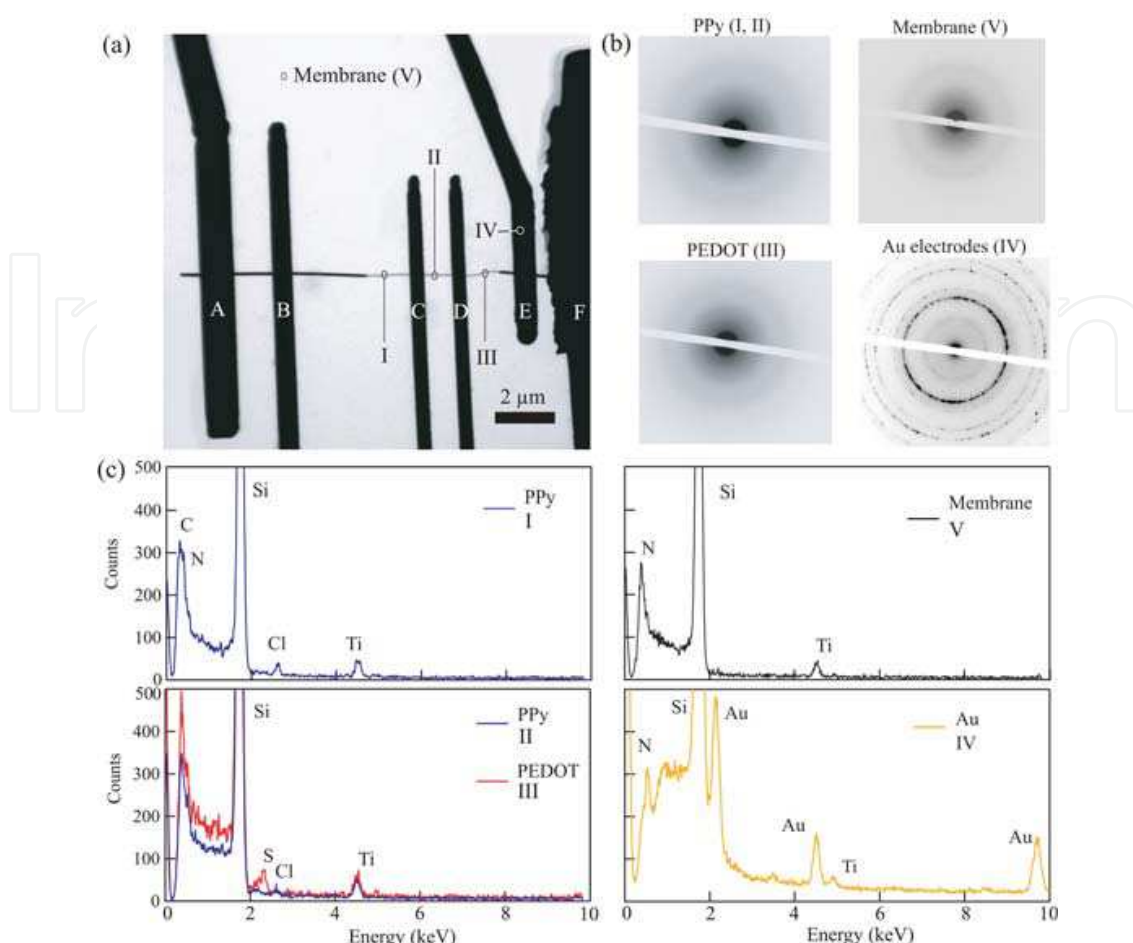
Fig. 14. (a) TEM picture of a Au-PEDOT-PPy-Au NW deposited on top of a silicon nitride membrane and connected with several electrodes. (b) Selected area electron diffraction patterns taken at three positions along the NW, membrane, and on top of the electrodes. (c) Energy dispersive X-ray spectra measured at four different positions on the device.

low PPy doping ratio generally observed in Au-PPy-Au NW [Gence (2007)]. More important, the data suggest that the Au-PEDOT and PPy-Au interfaces are not equivalent in terms of electrical conductivities. The Au-PPy interface presents a conductance roughly 30 times smaller than the Au-PEDOT interface. Therefore, electrical data analysis of hybrid metal-CP NWs requires utmost care: normally, the conductivities of the metallic segments and the associated metal-CP interfaces are much larger than the conductivities of the CP segments and the interfaces between two CPs. This, obviously, is not always the case. By illustrating this electrical dissymmetry of the metal-CP interfaces, the $I - V$ spectroscopy is heralded as the key component of the correlated characterization tool box that could enable the rational design of hybrid metal-CP NWs.

6. Integration and applications

The successful assembly of CP-based NWs into hierarchical structures is a key step necessary towards commercially attractive materials and devices. An illustrative example, sorted out from emerging niche applications, is molecular thermoelectricity. Innovative, low-cost thermoelectric converters, combining CPs and metals, could open new vistas in the
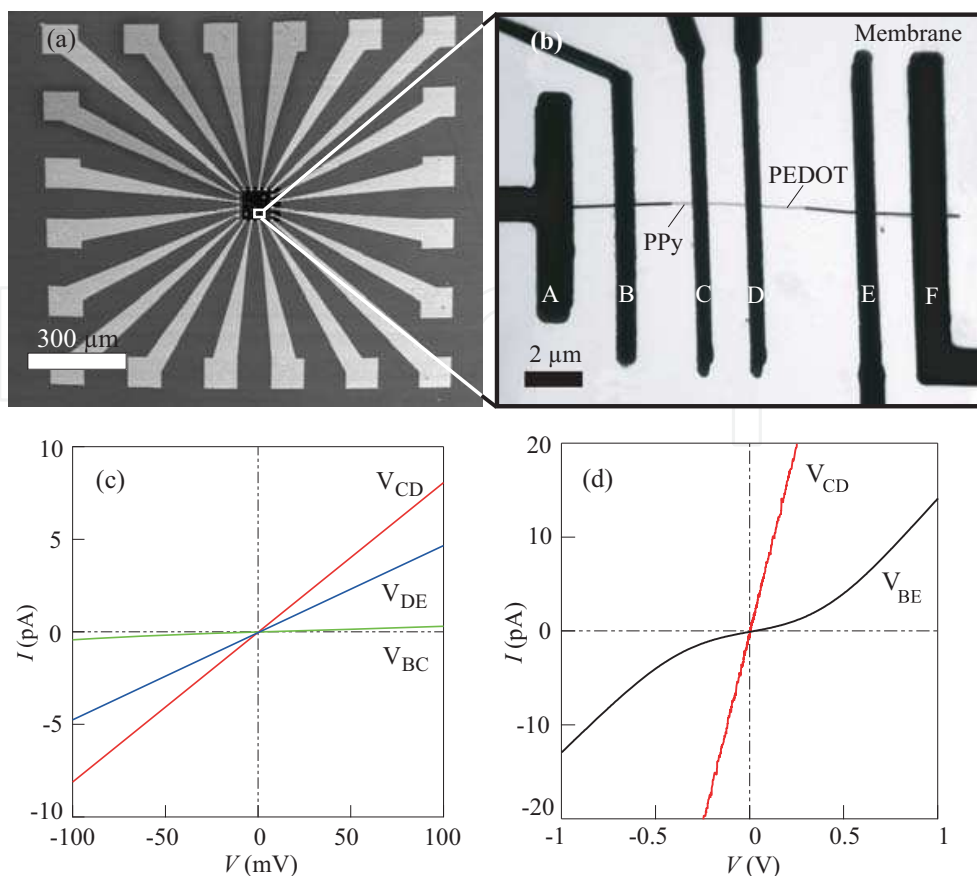
Fig. 15. (a) SEM picture of a membrane-based device used for the correlated characterization of a 110 nm diameter Au-PEDOT-PPy-Au NW. (b) TEM picture of the nanowire contacted with several electrodes. (c) $I - V$ characteristics of three different segments of the NW measured by the four-point technique. (d) Comparison of high bias $I - V$ characteristics of the NW segments BE (V_{BE}) and CD (V_{CD}). The resistance of the interfaces contributes to the higher resistance measured for the segment BE.

search for inexpensive sources of energy. Clearly, the level of integration depends on the envisaged applications; CP-based NWs, processed in mass quantities, are often incorporated in functional layers and they not require complex integration schemes. On one hand, CP designed as functional low-dimensional coatings of NWs or NTs [Lorcy (2009)] are following an easy way towards applications in life sciences (e.g. bio or chemical sensors). On the other hand, CP-based NWs used in electronic devices (e.g. flexible memory devices or thermoelectric converters), have to be integrated into a specific area of the device where physical, chemical or electrical interactions with the environment are permitted. This integration means that NWs have to be manipulated individually and placed on specific sites. Many techniques based on the use of the electric or magnetic field, fluidic flow or chemical assembly have been proposed for addressing the integration of template synthesized NWs. Interestingly, this integration can be achieved by combining classical top-down and template methods. Precisely, it consists in synthesizing the NWs directly on the final device, where they are requested. In this respect, recent work has demonstrated that PANI NWs can be polymerized within PMMA templates [Yunus et al. (2009); Vlad (2009)] in both planar and vertical architectures.
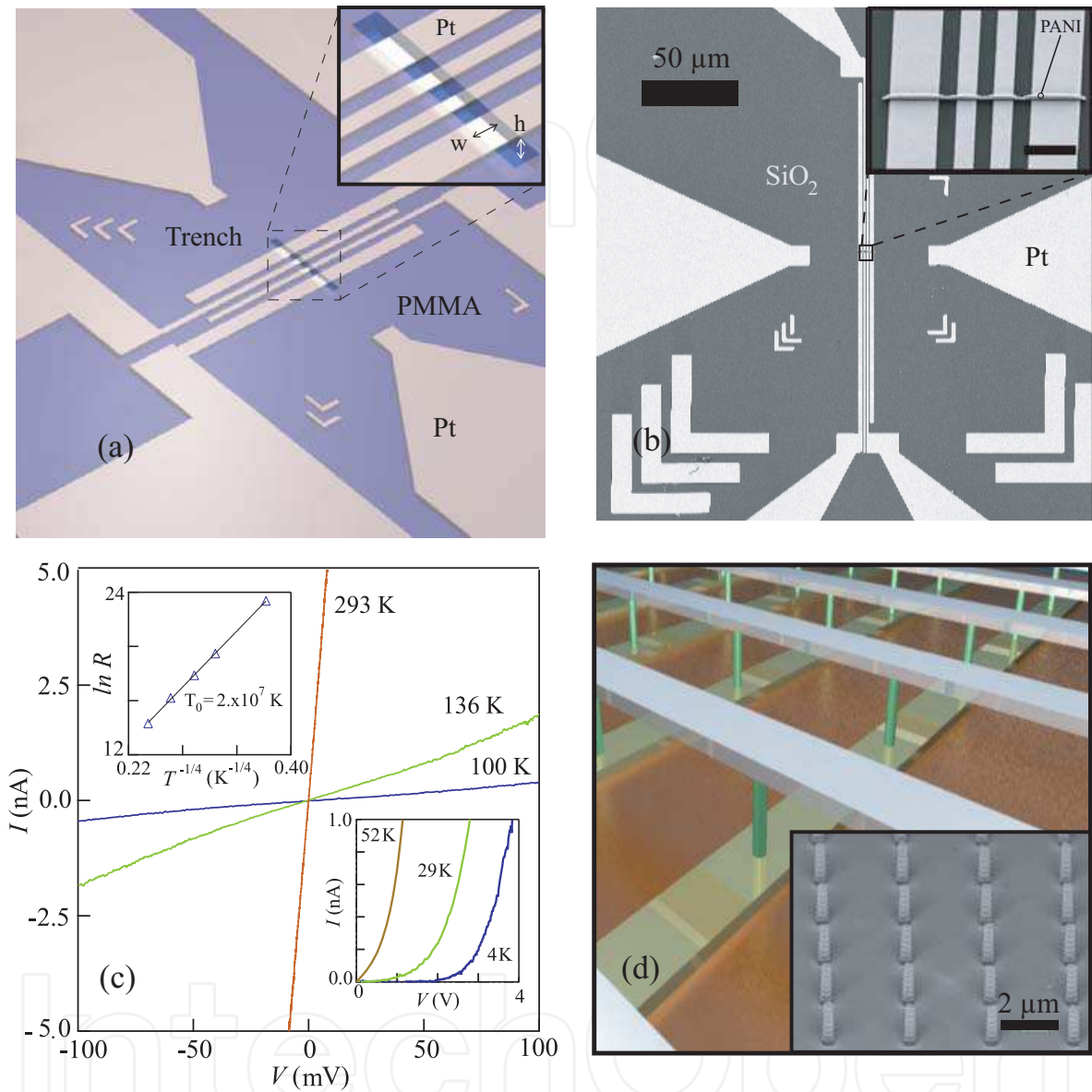
Fig. 16. (a) 3D schematic view of a PMMA template defined on top of four Pt electrodes. (b) SEM image of Pt electrodes used for synthesizing a single PANI NW defined within a PMMA template. The scale bar is 50 μm. The inset gives a closer zoom of the NW obtained after template removal. The scale bar is 2 μm. (c) Temperature dependent $I - V$ characteristics of the single PANI NW shown in (a). The lower inset shows the low-T data. The upper inset gives a 3D-VRH plot of the resistance. (d) 3D view of a cross bar architecture using single PANI NWs as active elements. The inset is a SEM picture of a highly ordered array of PANI NWs with diameter modulations.

Figure 16.(a) is a schematic view of a PMMA template defined on top of four Pt electrodes for planar NW integration. Here the template is created by EBL from a 500 nm thick PMMA layer; trenches are typically 200 nm wide and about 10 μm long. Figure 16.(b) presents a SEM micrograph of a device used for synthesizing a single PANI NW within a nano-engineered PMMA trench as a template and the inset offers a zoom on the NW after template removal. The temperature dependent $I - V$ characteristics of this PANI NW are given in Fig. 16.(c), revealing that the 3D VRH conduction regime dictates the charge transport in these planar integrated NWs, obtained via electroless polymerization.

In many cases, the bottom-up approach based on pure chemistry principles fails to reach extended, technologically relevant lengths for functional hybrid assemblies. On the contrary, hierarchical strategies employing standard Si manufacturing allow the achievement of a full superstructural control over the 3D spatial positioning of different self-assembled NWs for developing new artificial nanostructures. In this respect, femtomol-resolved polymerization of aniline on nano-engineered Pt reactors allows nano- and microscale device integration with single NW patterning and growth resolution. Figure 16.(d) offers a schematic view of a cross bar architecture for vertical integration of single PANI NWs as active elements [Vlad (2009)]. The inset displays a highly ordered array of PANI NWs with diameter modulations. The multiplexing feature included in these systems could be exploited for the controlled switching of individual NWs, while the peculiar morphology of the NWs could be adapted to plasmonics and photonics purposes.

A unique opportunity for macroscale self-assembly is offered by the structural engineering of CP-based NWs [Pokroy (2009)]. In a seminal paper, Park and co-workers, by controlling the dissolution of the template, created robust self-assembled mesoscopic metal-CP amphiphiles in which the segregated inorganic hydrophilic segments (Au), connected to the hydrophobic soft segments of the NWs (PPy), display unusual architectures such as bundles, tubes, and sheets [Park (2004)]. In fact, new and versatile functionalities of such hybrid architectures can be achieved easily by chemical treatment such as reversible acid-base doping-dedoping or redox reactions [He (2003); Chiou (2007); Vlad (2009)]. Another way to reach useful functionalities for CP-based NWs is to modify the CP segments by metallic nanoparticles. The figure 17.(a) gives a TEM image of a PEDOT NW functionalized by Au nanoparticles: the Au clusters are chemisorbed onto the PEDOT NW surface due to the presence of S atoms. Such modified NWs could be useful for biosensors applications [Tseng (2005)]. Furthermore, functionalities of CP architectures can be targeted by taking advantage of the peculiar morphology of the constituents. For instance, the axial modulation of aligned PANI NWs can be exploited to fabricate in a single step, self-aligned 3D arrays of vertically stacked Au nanorings (see Fig. 17.(b)).

7. Perspectives

Hybrid metal-CP NWs are promising high-tech materials - as they exhibit enhanced performances compared to their bulk counterparts [Hernandez (2004)] and are of direct interest for developing novel multifunctional systems for convergent micro-nano-bio-technology applications. Among many remaining challenges, we can mention 1) novel methodologies to fabricate highly-ordered architectures - for example, combining electroless and electrochemical depositions with self-assembly; 2) characterization strategies at nanoscale of hybrid NW based superstructures as demanded by molecular electronics, spintronics, plasmonics and photonics; 3) the use of CPs adaptive features for controlled
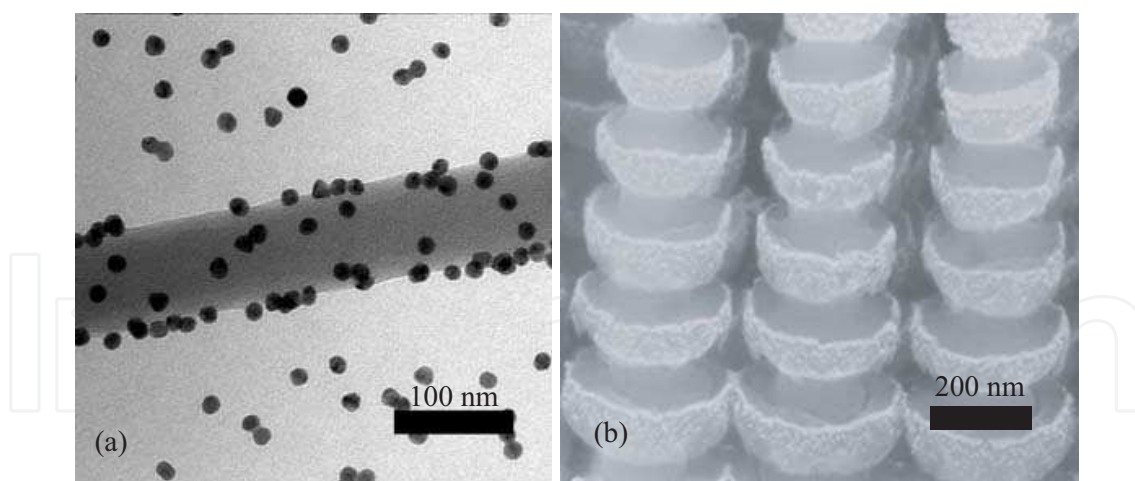
Fig. 17. (a) TEM picture of a single PEDOT NW functionalized by Au nanoparticles. The scale bar is 100 nm. (b) Au nanorings on PANI NWs obtained by physical evaporation through self-aligned stencil masks, provided here by the diameter modulations.

switching of device properties - at nanoscale - in the presence of external stimuli; 4) protocols for the manipulation of recognition properties of the constitutive segments towards engineering hybrid materials containing biomolecules like DNA or DNA/protein conjugates.

We are convinced that the greatest potential of electroactive CP-based NWs, by virtue of their responsiveness to magnetic, thermal and optical stimuli, is in interfacing the macroscopic world to the human physiological environment. Clearly, integrated hybrid metal- CP NWs into electrical impedance measurement platforms could prove highly beneficial in eliciting desired cellular responses with respect to biomolecules, including chemotaxis processes [Bagorda & Parent (2008)]. Relying on polypyrrole for exemplification, nanostructured 2D and 3D architectures with tunable electronic conductivity could be at the heart of interactive scaffolds that can be employed in tissue regeneration. As PPy has been extensively evaluated for various life science applications, encompassing amperometric biosensors, enzyme-based multicomponent electrodes in analyte detection systems [Li & Lin (2007)], or integrated DNA and peptide arrays on Si chips [Mailley et al. (2005)], there are now great prospects for the use of PPy-based NWs in high-tech applications, like enantiomeric sensing and chiral molecules separation [Huang et al. (2008)] or biocompatible nanoactuators [Lee (2008); Lim (2008)].

In conclusion, we believe that the challenges proposed here will bring new developments in the engineering of hybrid metal-CP NWs, together with the understanding of the mechanisms underlying a rational use of their molecular functions. In all likelihood, the combined efforts of engineers, chemists, and physicists will lead to breakthroughs in the development of artificial molecular recognition biosensor systems and opto-electronic applications.

8. Acknowledgements

9. References

Aguilar-Hernández, J. & Potje-Kamloth, K. (1999). Optical and electrical characterization of a conducting polypyrrole composite prepared by in situ electropolymerization, *Phys. Chem. Chem. Phys* 1: 1735–1742.

Aleshin, A. N. *et al*. (2004). One-dimensional transport in polymer nanofibers, *Physical Review Letters* 93(19): 196601.

Bagorda, A. & Parent, C. A. (2008). Eukaryotic chemotaxis at a glance, *J. Cell. Sci.* 121(16): 2621–2624.

Bearden, J. A. & Burr, A. F. (1967). Reevaluation of x-ray atomic energy levels, *Rev. Mod. Phys.* 39(1): 125–142.

Bufon, B. *et al*. (2005). Relationship between chain length, disorder, and resistivity in polypyrrole films, *The Journal of Physical Chemistry B* 109(41): 19191–19199.

Callegari, V. *et al*. (2009). Electrochemically template-grown multi-segmented gold-conducting polymer nanowires with tunable electronic behavior, *Chemistry of Materials* 21(18): 4241–4247.

Camposeo, A. *et al*. (2009). Laser emission from electrospun polymer nanofibers, *Small* 5(5): 562–566.

Cao, Y. *et al*. (2008). Electrical transport and chemical sensing properties of individual conducting polymer nanowires, *Nano Letters* 8(12): 4653–4658.

Chiou, N.-R. *et al*. (2007). Growth and alignment of polyaniline nanofibres with superhydrophobic, superhydrophilic and other properties, *Nature Nanotechnology* 2(6): 354–357.

Cho, S. I. & Lee, S. B. (2008). Fast electrochemistry of conductive polymer nanotubes: Synthesis, mechanism, and application, *Acc. Chem. Res.* 41(6):699-707.

Chtanko, N. *et al*. (2004). Etched single-ion-track templates for single nanowire synthesis, *The Journal of Physical Chemistry B* 108(28): 9950.

Chung, H.-J. *et al*. (2005). Cobalt-polypyrrole-cobalt nanowire field-effect transistors, *Applied Physics Letters* 86(21): 213113.

Dong, L. *et al*. (2005). Dielectrophoretic manipulation and electrical characterization of gold nanowires, *Nanotechnology* 16: 1500–1505.

Duvail, J. L. *et al*. (2002). Charge carrier transport in organic semiconductors, *Synthetic Metals* 131: 123.

Duvail, J. L. *et al*. (2004). Effects of the confined synthesis on conjugated polymer transport properties, *The Journal of Physical Chemistry B* 108(48): 18552–18556.

Duvail, J. L. *et al*. (2007). Tuning electrical properties of conjugated polymer nanowires with the diameter, *Applied Physics Letters* 90(10): 102114.

Duvail, J. L. *et al*. (2008). Physical properties of magnetic metallic nanowires and conjugated polymer nanowires and nanotubes, *International Journal of Nanotechnology* 5(6): 838–850.

Gence, L. *et al*. (2007). Structural and electrical characterization of hybrid metal-polypyrrole nanowires, *Physical Review B (Condensed Matter and Materials Physics)* 76(11): 115415.

Gence, L. *et al*. (2008). Size related transport mechanisms in hybrid metal-polymer nanowires, *Physica Status Solidi (a)* 205(6): 1447–1450.

Guo, Y. *et al*. (2008). Light-controlled organic/inorganic p-n junction nanowires, *Journal of the American Chemical Society* 130: 9198.

He, H. X. (2003). Discrete conductance switching in conducting polymer wires, *Phys. Rev. B* 68(4): 045302.

He, H. X., Li, C. Z. & Tao, N. J. (2001). Conductance of polymer nanowires fabricated by a combined electrodeposition and mechanical break junction method, *Applied Physics Letters* 78(6): 811–813.

Heremans, J. P. *et al*. (2002). Thermoelectric power of bismuth nanocomposites, *Phys. Rev. Lett.* 88(21): 216801.

Heremans, J. P. *et al*. (2003). Resistance, magnetoresistance, and thermopower of zinc nanowire composites, *Phys. Rev. Lett.* 91(7): 076804.

Hernandez, R. M. *et al*. (2004). Template fabrication of protein-functionalized gold-polypyrrole-gold segmented nanowires, *Chemistry of Materials* 16(18): 3431.

Huang, J., Wei, Z. & Chen, J. (2008). Molecular imprinted polypyrrole nanowires for chiral amino acid recognition, *Sensors and Actuators B: Chemical* 134(2): 573 – 578.

Hurst, S. J. *et al*. (2006). Multisegmented one-dimensional nanorods prepared by hard template synthetic methods, *Angew. Chem. Intl. Ed.* 45(17): 2672–2692.

Jang, J. (2006). Conducting polymer nanomaterials and their applications, *Adv Polym Sci.* 199: 189–259.

Jerôme, C. & Jerôme, R. (1998). Electrochemical synthesis of polypyrrole nanowires, *Angew. Chem. Intl. Ed.* 37(18): 2488.

Kovtyukhova, N. *et al*. (2004). Coaxially gated in-wire thin-film transistors made by template assembly, *Journal of the American Chemical Society* 126(40): 12738.

Lahav, A. *et al*. (2006). Core-shell and segmented polymer-metal composite nanostructures, *Nano Letters* 6(9): 2166.

Lee, J. I. *et al*. (2008). Highly aligned ultrahigh density arrays of conducting polymer nanorods using block copolymer templates, *Nano Letters* 8(8): 1530.

Li, J. & Lin, X. (2007). Glucose biosensor based on immobilization of glucose oxidase in poly(o-aminophenol) film on polypyrrole-Pt nanocomposite modified glassy carbon electrode, *Biosensors and Bioelectronics* 22(12): 2898–2905.

Liang, L. *et al*. (2002). Highly diastereo- and enantioselective intramolecular amidation of saturated C-H bonds catalyzed by ruthenium porphyrins, *Angewandte Chemie International Edition* 41(18): 3465.

Lieber, C. M. & Wang, Z. L. (2007). Functional nanowires, *MRS Bulletin* 32(3): 99.

Lim, J.-H. & Mirkin, C. A. (2002). Electrostatically driven dip-pen nanolithography of conducting polymers, *Advanced Materials* 14(20): 1474–1477.

Lim, J. K. *et al*. (2008). Actuation of self-assembled two-component rodlike nanostructures, *Nano Letters* 8(12): 4441.

Long, Y. *et al*. (2005). Electronic transport in single polyaniline and polypyrrole microtubes, *Phys. Rev. B* 71(16): 165412.

Lorcy, J.M. *et al*. (2009). Coaxial nickel/poly(p-phenylene vinylene) nanowires as luminescent building blocks manipulated magnetically, *Nanotechnology* 20(40): 405601.

Mailley, P., Roget, A. & Livache, T. (2005). Conducting polymers for DNA sensors and DNA chips: from fabrication to molecular detection, Persp. In Bioanalysis 1: 297–330.

Martin, C. R. (1994). Nanomaterials: A membrane-based synthetic approach, *Science* 266(5193): 1961–1966.

Martin, C. R. (1996). Membrane-based synthesis of nanomaterials, *Chemistry of Materials* 8(8): 1739.

Massuyeau, F. *et al*. (2009). Elaboration of conjugated polymer nanowires and nanotubes for tunable photoluminescence properties, *Nanotechnology* 20(15): 155701.

Merlo, J. A. & Frisbie, C. D. (2004). Field effect transport and trapping in regioregular polythiophene nanofibers, *J. Phys. Chem. B* 108:19169.

Mott, N. F. & Davis, E. A. (1979). *Electronic Processes in Non-Crystalline Materials*, Clarendon Press, Oxford.

Nalwa, H. S. (ed.) (2006). *Polymeric Nanostructures and Their Applications*, American Scientific Publishers.

Park, S. *et al.* (2004). Hybrid organic-inorganic, rod-shaped nanoresistors and diodes, *Journal of the American Chemical Society* 126: 11772.

Pinto, N. J. *et al.* (2003). Electrospun polyaniline/polyethylene oxide nanofiber field-effect transistor, *Applied Physics Letters* 83(20): 4244–4246.

Pinto, N. J. *et al.* (2009). Rectifying junctions of tin oxide and poly(3-hexylthiophene) nanofibers fabricated via electrospinning, *Applied Physics Letters* 94(8): 083504.

Pokroy, B. *et al.* (2009). Self-organization of a mesoscale bristle into ordered, hierarchical helical assemblies, *Science* 323(5911): 237–240.

Reneker, D. H. *et al.* (2000). Bending instability of electrically charged liquid jets of polymer solutions in electrospinning, *Journal of Applied Physics* 87(9): 4531–4547.

Reynes, O. & Demoustier-Champagne, S. (2005). Template electrochemical growth of polypyrrole and gold-polypyrrole-gold nanowire arrays, *Journal of The Electrochemical Society* 152(9): D130–D135.

Sadki, S. *et al.* (2000). The mechanisms of pyrrole electropolymerization, *Chem. Soc. Rev.* 29: 283.

Sakmeche, N. *et al.* (1996). Anionic micelles: a new aqueous medium for electropolymerization of poly(3,4-ethylenedioxythiophene) films on Pt electrodes, *Chem. Commun.* pp. 2723–2724.

Shen, J. *et al.* (2006). Electrical properties of a single electrochemically template-synthesized polypyrrole nanowire, *Applied Physics Letters* 88(25): 253106.

Smith, P. A. *et al.* (2000). Electric-field assisted assembly and alignment of metallic nanowires, *Applied Physics Letters* 77(9): 1399–1401.

Tran, H. D., Li, D.& Kaner, R. B. (2009). One-dimensional conducting polymer nanostructures: Bulk synthesis and applications, *Advanced Materials* 21(1): 1–13.

Tseng, R. J. *et al.* (2005). Polyaniline nanofiber/gold nanoparticle nonvolatile memory, *Nano Letters* 5(6): 1077.

Vlad, A. *et al.* (2009). Highly ordered conjugated polymer nanoarchitectures with three-dimensional structural control, *Nano Letters* 9(8): 2838 – 2843.

Wan, M. (2008). A template-free method towards conducting polymer nanostructures, *Advanced Materials* 20(15): 2926–2932.

Wang, J. G. *et al.* (2004). Microstructure and interdiffusion of template-synthesized Au/Sn/Au junction nanowires, *Nano Letters* 4(7): 1313.

Wang, Y. *et al.* (2007). Individually addressable crystalline conducting polymer nanowires in a microelectrode sensor array, *Nanotechnology* 18(42): 424021.

Xiao, R. *et al.* (2007). Controlled electrochemical synthesis of conductive polymer nanotube structures, *Journal of the American Chemical Society* 9(3): 40–50.

Yoon, C. O. *et al.* (1994). Transport near the metal-insulator transition: Ppy doped with PF_6, *Phys. Rev. B* 49(16): 10851–10863.

Yoon, H., Hong, J.-Y. & Jang, J. (2007). Charge-transport behavior in shape-controlled poly(3,4-ethylenedioxythiophene) nanomaterials: Intrinsic and extrinsic factors, *Small* 3(10): 1774–1783.

Yunus, S., Attout, A. & Bertrand, P. (2009). Controlled aniline polymerization strategies for polyaniline micro- and nano self-assembling into practical electronic devices, *Langmuir* 25(3): 1851.

Nanowires Science and Technology

Edited by Nicoleta Lupu

This book describes nanowires fabrication and their potential applications, both as standing alone or complementing carbon nanotubes and polymers. Understanding the design and working principles of nanowires described here, requires a multidisciplinary background of physics, chemistry, materials science, electrical and optoelectronics engineering, bioengineering, etc. This book is organized in eighteen chapters. In the first chapters, some considerations concerning the preparation of metallic and semiconductor nanowires are presented. Then, combinations of nanowires and carbon nanotubes are described and their properties connected with possible applications. After that, some polymer nanowires single or complementing metallic nanowires are reported. A new family of nanowires, the photoferroelectric ones, is presented in connection with their possible applications in non-volatile memory devices. Finally, some applications of nanowires in Magnetic Resonance Imaging, photoluminescence, light sensing and field-effect transistors are described. The book offers new insights, solutions and ideas for the design of efficient nanowires and applications. While not pretending to be comprehensive, its wide coverage might be appropriate not only for researchers but also for experienced technical professionals.

How to reference

In order to correctly reference this scholarly work, feel free to copy and paste the following:

L. Gence, V. Callegari, S. Melinte, S. Demoustier-Champagne, Y. Long, A. Dinescu and J.L. Duvail (2010). Conjugated Polymer and Hybrid Polymer-Metal Single Nanowires: Correlated Characterization and Device Integration, Nanowires Science and Technology, Nicoleta Lupu (Ed.), ISBN: 978-953-7619-89-3, InTech, Available from: http://www.intechopen.com/books/nanowires-science-and-technology/conjugated-polymer-and-hybrid-polymer-metal-single-nanowires-correlated-characterization-and-device-

INTECH

open science | open minds